



*"The project has received funding from the European Union's Horizon 2020 research and innovation programme under grant agreement No 723205"*

## **Deliverable D3.3**

# **Guidelines for installation of smart sensors for monitoring of LC infrastructure**

**Due date of deliverable: 30/04/2019**

**Actual submission date: 09/06/2020**

### **Authors:**

Delphine Jacqueline and Raphael Antoine, (Cerema)

Elias Kassa (NTNU)

© Copyright 2017 SAFER-LC Project (project funded by the European Commission). All rights reserved.

No part of this document may be copied, reproduced, disclosed or distributed by any means whatsoever, including electronic without the express permission of the International Union of Railways (UIC), Coordinator of the EU SAFER-LC Project. The same applies for translation, adaptation or transformation, arrangement or reproduction by any method or procedure whatsoever.

The document reflects only the author's views and neither INEA nor the Commission is liable of any use that may be made of the information contained therein. The use of the content provided is at the sole risk of the user.

## Project details

Project acronym	SAFER-LC
Project full title	SAFER Level Crossing by integrating and optimizing road-rail infrastructure management and design
Grant Agreement no.	723205
Call ID and Topic	H2020-MG-2016-2017, Topic MG-3.4-2016
Project Timeframe	01/05/2017 – 30/04/2020
Duration	36 Months
Coordinator	UIC – Marie-Hélène Bonneau (bonneau@uic.org)

## Document details

Title	Guidelines for installation of smart sensors for monitoring of LC infrastructure
Work Package	WP3
Date of the document	09/06/2020
Version of the document	07
Responsible partner	NTNU - CEREMA
Reviewing partner	Cerema, RWTH, UIC
Status of the document	Final
Dissemination level	Public

## Document history:

Revision	Date	Description
01	14/06/2019	First draft prepared by NTNU and CEREMA
02	30/10/2019	Second draft circulated after reviewed by CEREMA
03	01/05/2020	Third draft circulated
04	02/06/2020	Final version for submission after reviewed by RWTH
05	04/06/2020	Final review by UIC
06	08/06/2020	Final review by NTNU
07	09/06/2020	Ethical and final review

## Consortium - List of partners

Partner No	Short name	Name	Country
1	UIC	International Union of Railways	France
2	VTT	Teknologian tutkimuskeskus VTT Oy	Finland
3	NTNU	Norwegian University of Science and Technology	Norway
4	IFSTTAR	French institute of science and technology for transport, development and networks	France
5	FFE	Fundación Ferrocarriles Españoles	Spain
6	CERTH-HIT	Centre for Research and Technology Hellas - Hellenic Institute of Transport	Greece
7	TRAI NOSE	Trainose Transport – Passenger and Freight Transportation Services SA	Greece
8	INTADER	Intermodal Transportation and Logistics Research Association	Turkey
9	CEREMA	Centre for Studies and Expertise on Risks, Environment, Mobility, and Urban and Country planning	France
10	GLS	NeoGLS	France
11	RWTH	Rheinisch-Westfaelische Technische Hochschule Aachen University	Germany
12	UNIROMA3	University of Roma Tre	Italy
13	COMM	Commsignia Ltd	Hungary
14	IRU	International Road Transport Union - Projects ASBL	Belgium
15	SNCF	SNCF	France
16	DLR	German Aerospace Center	Germany
17	UTBM	University of Technology of Belfort-Montbéliard	France

## Executive Summary

Deliverable D3.3 is the third deliverable of the Work Package 3 (WP3). This deliverable aims to deliver guidelines for installation of smart sensors to monitor an LC infrastructure (task 3.3). Within this context, two main measurement systems are developed, installed, and evaluated. In addition, further measurements are conducted to assess other parts of the LC infrastructure. The main objective is to assess the condition of LC infrastructure which may have safety risks for LC users and to identify LC profiles that may risks road vehicles being stuck due to the LC design faults, construction wrong profile or deterioration of the different layers of the LC structure.

Level crossings may have either passive or active protection which change its state (sound, light or mechanical barrier). The normal operation of these protections is inspected and maintained regularly. Any functional failure or wrong operation of these systems should be inspected and maintained. Failure to inspect and maintain these infrastructures may cause accidents at LC. The roadbed of the LC should normally be inspected. Poor maintenance and deterioration of the LC structure may result in bumpiness and very rough LC surface which may result in drivers losing control of their vehicles leading to a crash. In some cases, the vertical profile design of the LC may lead to a conflict point with low-profile vehicles crossing the LC. Such design and construction fault may lead to conflicting point leading to a safety concern and/or closure of the LC and delays associated to it.

This document provides how the different measurement techniques are used to monitor the surface profile and displacement of the road surface and to measure vibration of the track/road component due to dynamic loading of passing vehicle in real time. The measurements are used to identify conflict points and to set alert thresholds to assess the status of the LC components and to send these alerts to LC owners and maintainers of possible safety risk. Further, the LC barrier boom is monitored to identify and predict any potential failure or malfunction as well as traffic signal light operational functionality.

## Table of contents

<b>1. Introduction .....</b>	<b>7</b>
1.1 Objectives of the SAFER-LC project.....	7
1.2 Objectives of the Task 3.3 .....	7
1.3 Purpose of this deliverable.....	8
1.4 Interactions with other tasks and workflow of the project .....	9
1.5 Structure of the document.....	9
1.6 Acronyms .....	10
<b>2. Description of the work.....</b>	<b>11</b>
2.1 Accidents at Level crossing .....	12
2.2 Level crossings protection types.....	14
2.3 Conflict points .....	15
<b>3. Experimental test site .....</b>	<b>17</b>
3.1 Implementation .....	17
3.2 Test site configurations .....	19
3.2.1 Bump configurations .....	19
3.2.2 Hollow configurations.....	20
3.3 Measurements used to detect surface degradations.....	23
3.3.1 Photogrammetric method .....	23
3.3.2 Vibration.....	24
3.3.3 Thermoinfrared .....	28
3.3.4 Equipped vehicle of Cerema (VACC) .....	28
3.4 Scenarios used in the measurements .....	29
<b>4. Description of the photogrammetric method.....</b>	<b>31</b>
4.1 Choice of the photogrammetric method in the SAFER-LC project.....	31
4.2 Material description.....	31
4.3 Settings definition .....	35
4.4 Settings of the cameras .....	37
4.5 Description of the photogrammetric data processing .....	38
<b>5. Description of the Vibration measurement method .....</b>	<b>40</b>
5.1 Vibration measurement.....	40
5.2 Accelerometers data processing .....	41
5.3 Alert threshold levels definition .....	42

5.3.1	Warning and Danger levels for a LC .....	43
5.4	Data analysis.....	45
5.4.1	Vibration data in time domain .....	45
5.4.2	PSD analysis .....	47
6.	<b><i>LC Barrier and Traffic light monitoring method</i></b> .....	<b>53</b>
6.1	Automatic control system.....	53
6.2	Level Crossing Motor Current Analysis .....	55
6.3	Traffic signal light current measurement .....	57
7.	<b><i>Preliminary results for chosen scenarios</i></b> .....	<b>59</b>
7.1	Photogrammetry .....	59
7.2	Vibration (VACC, seismic) .....	64
7.3	The thermal infrared method: a tool complementary to photogrammetry.....	66
8.	<b><i>Conclusions and next steps</i></b> .....	<b>72</b>
9.	<b><i>Bibliography</i></b> .....	<b>74</b>

## 1. INTRODUCTION

---

### 1.1 Objectives of the SAFER-LC project

The main objective of the SAFER-LC project is to improve safety and minimise risks at and around level crossings (LCs) by developing a fully integrated cross-modal set of innovative solutions and tools for the proactive management and new design of level-crossing infrastructure. These tools will enable:

- i. Road and rail decision makers to achieve better coherence between both modes,
- ii. Effective ways to detect potentially dangerous situations leading to collisions at LCs as early as possible,
- iii. The prevention of incidents and accidents at level crossing through innovative design and predictive maintenance methods, and
- iv. The mitigation of the consequences of incidents/disruptions due to accidents or other critical events.

The main output of the SAFER-LC project is a toolbox which is accessible through a user-friendly interface while integrating all the project results and solutions to help both road and rail stakeholders to improve safety at level crossings.

The project focuses both on technical solutions and on human processes to adapt infrastructure designs to road user needs and to enhance coordination and cooperation between different stakeholders from different land transportation modes. The challenge is also to demonstrate the acceptance of the proposed solutions by both road and rail users and to implement the solutions cost-efficiently.

### 1.2 Objectives of the Task 3.3

Within the project, the objective of Work Package3 (WP3) is to develop technological solutions to improve safety at level crossings as well as at working zones through sharing information and giving warnings to trains/vehicles approaching/arriving to level crossings and to workers at or near train passing zones. The solutions developed in this WP are components for the SAFER-LC toolkit. This deliverable (D3.3) focusses on developing and evaluating different technologies for monitoring of LC infrastructure.

The objective of Task 3.3 is to develop an automated and real-time system to monitors the condition of LCs using sensors on the track and roadside. Recommendations from WP1 has been used to determine the LC infrastructure to be monitored, and the type of data and the type of sensors to be used for the monitoring purpose. Through the data gathered by the sensors, the aim is to assess the conditions of the LC infrastructure and to suggest proactive maintenance approach for the LC. It also aims to increase the reliability of the infrastructure through the continuous and real time monitoring and hence improves the Life Cycle Cost.

The monitoring system includes continuous and real time inspection through two approaches:

- by use of vibration sensors installed on the relevant track/road components and data transmitted with an alert threshold to the LC operator. The system enables to send alerts to LC users; and
- by use of photogrammetric device to monitor infrastructure surface condition and detect any deterioration of the structure. This system also measures displacement and deterioration of the road surface. In addition, this visible information to be combined with thermal infrared data to enhance the interpretations of the potential disorders as cracking.

### **1.3 Purpose of this deliverable**

This deliverable reports on the work conducted in Task 3.3 of WP3 with the objective to develop an automated real-time system to monitors the condition of LCs using sensors on the track and roadside.

It describes how the different measurement techniques are used to monitor the surface profile and displacement of the road surface and to measure vibration of the track/road component due to dynamic loading of passing vehicle in real time on mock-up structure built in an experimental test site in France. The measurements are used to identify conflict points and to set alert thresholds to assess the status of the LC components and to send these alerts to LC owners and maintainers of possible safety risk. It aims to detect infrastructure conditions (and any deterioration of the structure) to avoid collisions at LCs between trains and heavy vehicles stuck at LCs. The original objective was to use smart and embedded wireless sensor networks to collect vibration data from passing vehicle on the LC. However, due to professional expertise developing the system leaving the project team, the implementation of wireless sensor has been dropped and commercially available wired vibration sensors has been implemented in the test site to collect vibration data.

The issue of vehicles stuck at LCs relates to the longitudinal section on either side of the LC. Railway managers have a topographic section with a lower level of accuracy. The photogrammetric method improves the detection of dangerous profiles through measurement of displacement and deterioration of the road surfaces. Further, the LC barrier boom is monitored to identify and predict any potential failure or malfunction as well as traffic signal light operational functionality.



## 1.4 Interactions with other tasks and workflow of the project

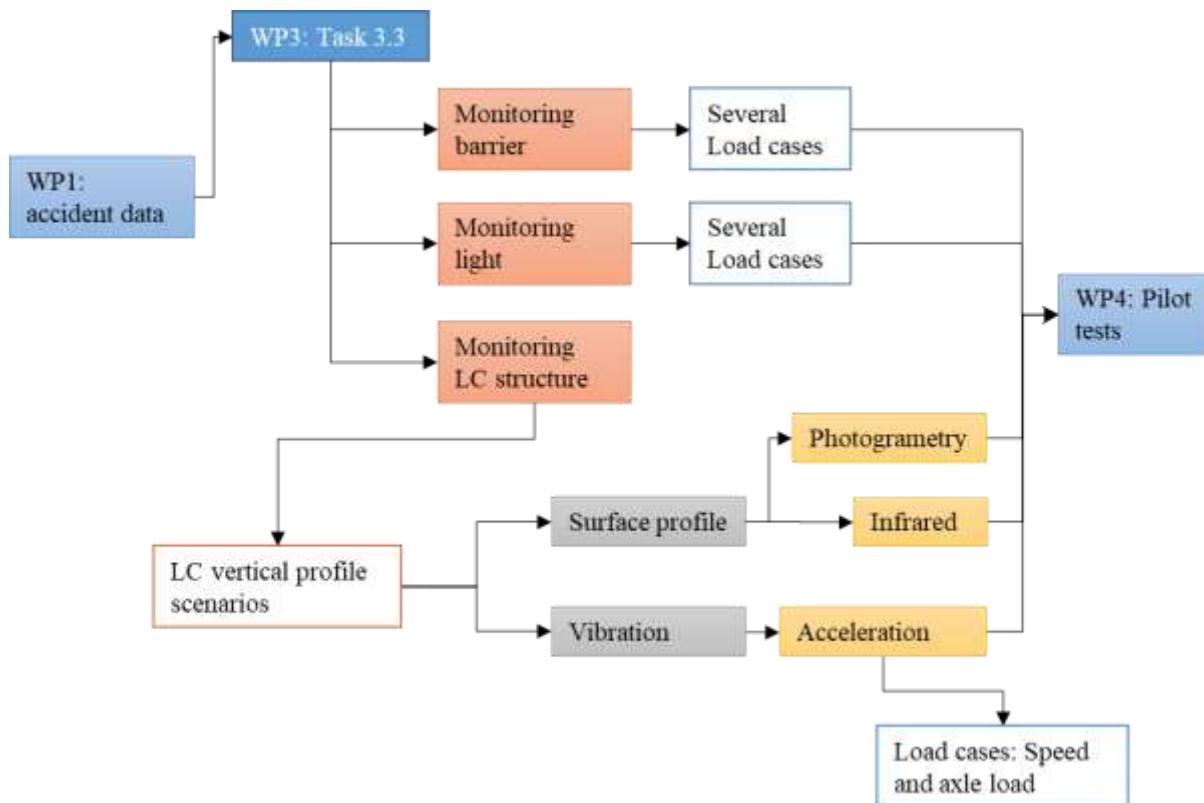


Figure 1. Workflow of Task 3.3 and interaction with other WPs and tasks.

The workflow for the task is shown in Figure 1. The task has direct link with WP1 and WP4. The work included in this deliverable are: barrier function monitoring, signal light monitoring and LC structure monitoring with several vertical profile scenarios. Safety risk scenarios identified in WP1 has been used as an input in this deliverable.

## 1.5 Structure of the document

Section 1 details general introduction and description of the deliverable. Objective of the test site configurations, implementation and measurements used are discussed in Section 2. Section 3 contains the description of the Photogrammetric method while section 4 contains description of the vibration method. In section 5, the barrier motor and traffic light monitoring methods is given, which is followed by section 6 discussing some of the results of chosen scenarios. The last section contains conclusion and future works.

## 1.6 Acronyms

Abbreviation	Description
ADC or A/D	Analog to Digital Converter
AASHTO	American Association of State Highway and Transportation Officials
AEL	Auto Exposure Lock
AREMA	American Railway Engineering and Maintenance-of-Way Association
CECP	“Centre d’Etudes et de Construction de Prototypes” in French of Cerema (Studies and Prototype Design Center)
CER	“Centre d’Expérimentation et de Recherche” in French of Cerema (Experimental and Research Center)
CBM	Condition-based maintenance
DJI	Da Jiang Innovation (drone constructor)
FLIR	Forward Looking InfraRed
FRA	Federal Railroad administration
GCP	Ground Control Point (in micmac software)
GPS	Global Positioning System
HD	High Definition
IEEE	Institute of Electrical and Electronics Engineers
ISBN	International Standard Book Number
ISO	International Organization for Standardization
ISPRS	International Society for Photogrammetry and Remote Sensing
LC	Level Crossing
LiDaR	Light Detection and Ranging
M3C2	Multiscale Model to Model Cloud Comparison (in micmac software)
PLaS	Photogrammetry-based method for LAndSlide Study
Std	Standard Deviation
UAV	Unmanned Aerial Vehicle
VACC	Véhicule d’Analyse du Comportement des Conducteurs” in French
WP	Work Package
WSN	Wireless sensor networks

## 2. DESCRIPTION OF THE WORK

Level crossing (LC) is an infrastructure whereby road vehicles and railway vehicles intersect each other's track at the same grade. From 1839, the railway company introduced safety measures as well as standardization for public level crossings. To facilitate a smooth crossing of vehicles as well as other level crossing users where they cross in the same grade, a number of infrastructures exist. The rail track for running trains, approaching road pavement, crossing material of concrete or rubber, traffic light, barrier boom with machine, sound warnings, see Figure 2 and Figure 3.

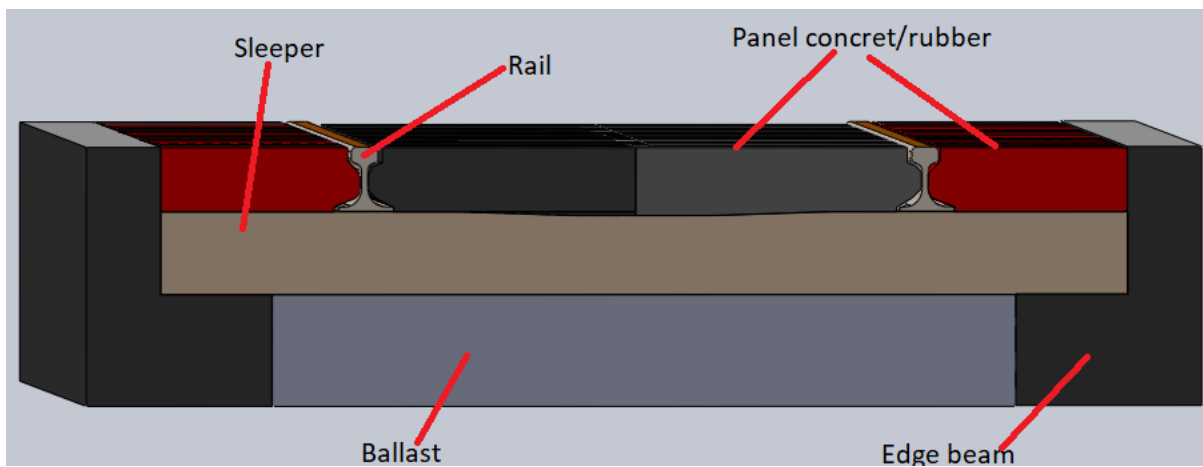


**Figure 2 :** *Level crossings and its components.*



**Figure 3.** *Level crossing with Strail material and approaching road (left), active level crossing with traffic lights and barrier gates (right).*

## 2.1 Accidents at Level crossing

The rail-road level crossing is a problematic junction for the two modes affecting both safety and rideability. Bumpiness, steep grades, sagging vertical profile, poor surface quality, all these surface profile features increase risk of collision for long and big trailers and busses with trains. Low profile vehicles may also stuck in level crossings leading to a risk of being smashed by oncoming trains, see Figure 4. An accident occurred due to a heavy goods track stucked on tracks at level crossings leading to a crash with a train where two people died and 18 injured [1], see Figure 5. While crashes at LCs shows a decreasing trend, there is still a considerable amount of accidents. Some of the accidents are related with the deterioration of the LCs and the vertical profile having conflict with long and low-level trailers, see Figure 6.



**Figure 4 :** A heavy duty truck Stacked on a level crossings and was hit by a train in the US state of Georgia [1].

There are about 120,000 number of LCs in the whole Europe, on average there are 4 level crossings in each 10 km section of track [2]. Maintaining and auditing the condition of such a huge number of infrastructure is a challenging task for infrastructure owners. Personal visit of the infrastructure is the main inspection method, which requires significant amount of human resource and cost. According to Federal Railroad administration (FRA) statistics, 2,217 road-rail LC collisions occurred in 2018, leading to over 260 deaths and much higher number of serious injuries [3]. Hence, from the safety point of view, level crossings are critical points in the safe operation of the rail infrastructure. Statistical analysis of accidents shows that the main cause of all accidents is the human factor of road users. [4].



**Figure 5 :** *A local train smashed into the heavy goods vehicle in Italy [5].*



**Figure 6 :** *Aftermath of a hump crossing collision [6].*

Poor maintenance and deterioration of the LC infrastructure may result in bumpiness and very rough LC surface, see Figure 7. This uneven profile of the LCs may disrupt the normal driving of vehicles and may result in drivers losing control of their vehicles leading to a crash. In some cases, the rail track geometry and the track super elevation (cant) may dictate the LC geometry, leading to a vertical profile design, which may lead to a conflict point with low-profile vehicles, see Figure 8. Crossing safety due to such conflicting point has not been a main concern by road/rail authorities. However, recent accidents in Europe [2] and US [7] indicate that there is a safety concern and delays associated to it.



**Figure 7 :** *Potholes asphalt crossing surface*





**Figure 8 :** A truck passing a level crossing near Barcelona with bumpy profile

## 2.2 Level crossings protection types

Level crossings may have either passive or active protection. Passive protected level crossings are those crossings, which are equipped with any sign or warning devices or any other protection equipment that is constant and that does not change depending on any traffic situation. Whereas active protected level crossings are those with protection, which change its state (sound, light or mechanical barrier) according to the approaching train. Figure 3 shows a level crossing with active system. Risk evaluation due to road side and rail side causes are listed in the Deliverable 1.3 [8]. Some of the risk scenarios identified are related to malfunctioning of the barriers and barrier motor, failure on sound warning device and failure of signal lights. The normal operation of crossing barrier, traffic lights and sound bells should be inspected and maintained regularly. Failure to inspect and maintain these infrastructures may also be a cause for LC accidents. A passenger train smashed into a lorry in US where the crossing barriers, the lights and the bells fail to function, see Figure 9.

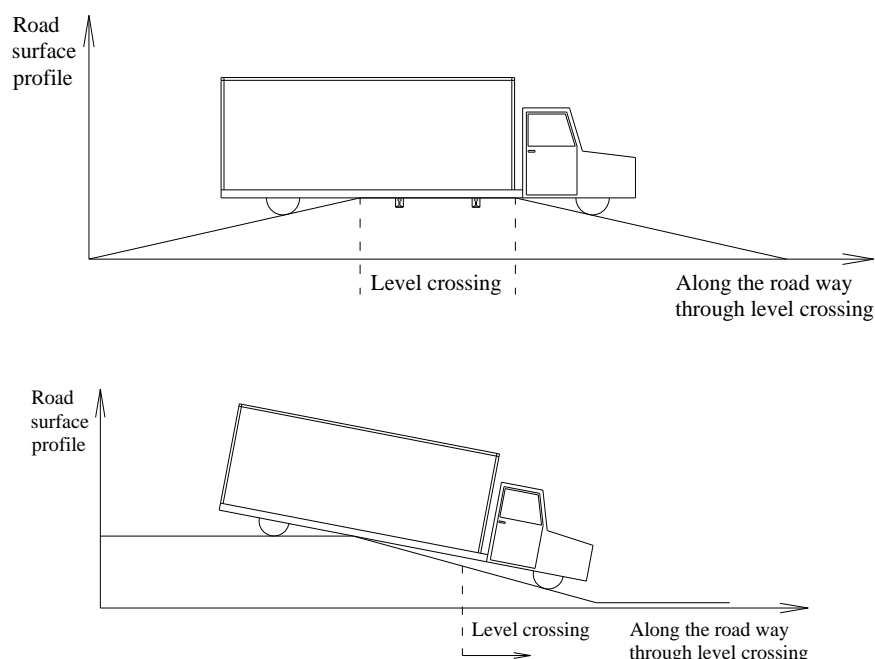


**Figure 9.** A passenger train violently smashed into a lorry in US [9].

## 2.3 Conflict points

Level crossing geometric design follows a guideline by national highway administrations, and the guide should take into consideration low-profile vehicles. Crossing geometric design guidelines are normally provided by highway and street design standards and the railway design guidelines. These standards guide to construct crossings to reduce or eliminate the probability of a vehicle becoming high-centered. The American design guides indicate that the surface of the highway should be neither more than 3 inches higher nor more than 6 inches lower than the top of the nearest rail at a point 30 feet from the rail, measured at a right angle, unless track super elevation dictates otherwise [10],[11].

Conflict points could arise due to design faults, constructions errors as well as deterioration of the sublayers under the LC structure. The vertical profile of the LC may lead to a conflict mainly with low floored lorries, buses, long trailers, etc. Figure 10 shows some graphical presentation of possible conflict points. Such profiles could be identified through the photogrammetric and comparing with trucks geometrical structure. However, the main objective of this work is to assess the vertical profile the LC due to deterioration of the road track leading to sagging and large deformation or humps, at which vehicles may have problems crossing the LC.



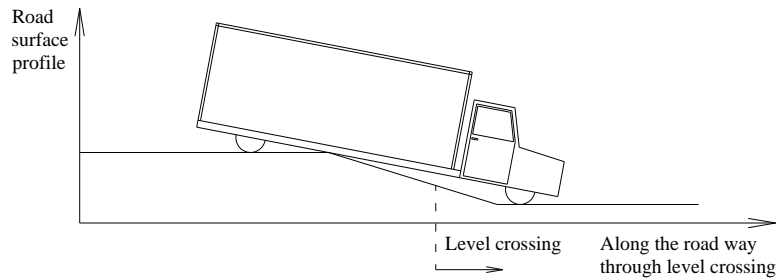


**Figure 10.** *Some graphical presentation of conflict points*

In winter and slippery weather, there might be also a problem for big lorries stopping before crossing the LC and to start and climb up the approaching road towards the LC. This may have a problem for starting power in slipper road condition. Large settlement of the LC material may also reveal to be a barrier to be climbed up by small cars. This may be a cause for small cars to be stuck and unable to climb the rail, especially if it is associated with steep gradient and cars start from stop at LCs. All these may be a cause for accidents. In this project, combined photogrammetric and vibration measurements try to identify such risks through vibration sensors for different car axle loads.



### 3. EXPERIMENTAL TEST SITE

---

The piloting of this measure was conducted at the Cerema experimental site in Normandy in the Experimental Research Centre. Cerema built an experimental semi level crossing with three meters of width (rubber system) to realize tests at full scale (Figure 11). The aim of the trial is to investigate the feasibility of different methods to detect degradation on level crossings.



**Figure 11.** Aerial view of the Cerema experimental site.

Two different road configurations – bump and hollow – were used to reproduce the most common types of natural relief road configurations (Figure 13).

#### 3.1 Implementation

The main aim is to test different methods and evaluate their feasibility to detect degradation on level crossings.

A LC structure was constructed in real conditions. All pieces have been ordered to build the rail panel in real conditions at a scale 1:1.

The implementation of the experimental LC structure (configuration a) is composed of 7 steps described in Figure 12.

The first image represents the digging for the location of the experimental LC. The second picture shows the drain to evacuate meteoric water and the third one shows the gravel layer

supporting level crossing system. Picture 4 below consists of the railway track panel installation, both pictures 5 and 6 the LC rubber system (strail) installation and the last photo (7) show the compaction of the cold asphalt layer to fill holes between rubber system and road.



**Figure 12.** *Experimental level crossing implementation (Cerema test site)*

### 3.2 Test site configurations

The level crossing mock-up installed on Cerema experimental site will provide two types of road configurations (configuration 1 : bump and configuration 2 : hollow on Figure 13 below) to detect the infrastructure condition of LCs (e.g. degradation) by using sensors on equipped vehicles, track and road structure.

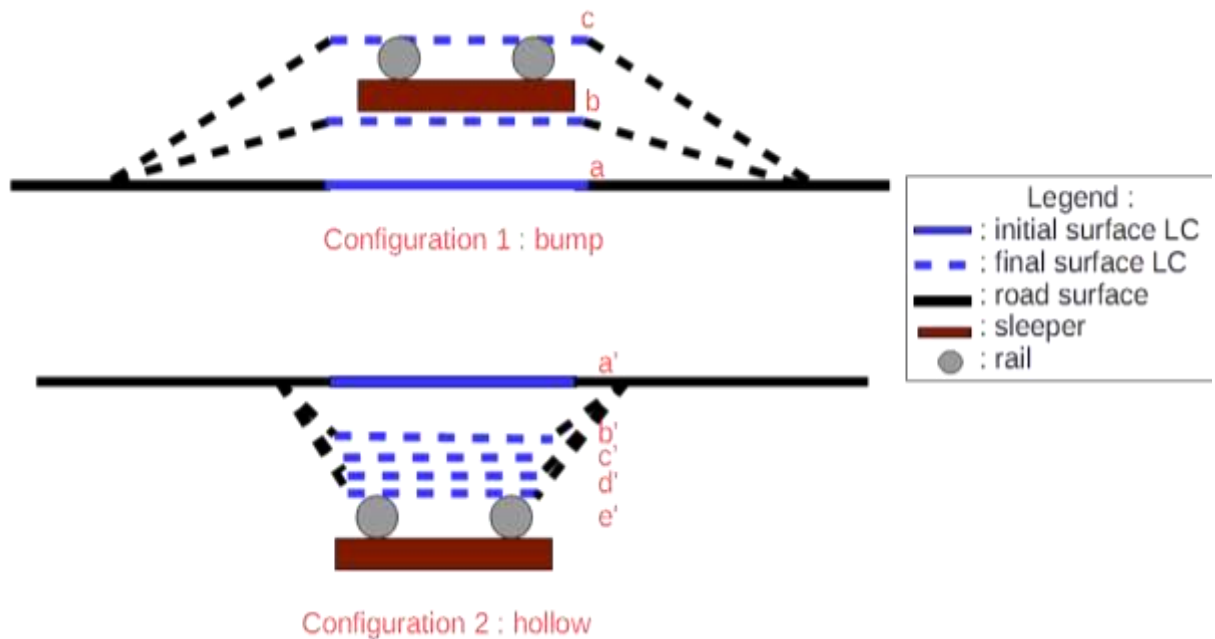


**Figure 13.** Different configurations of the Cerema experimental test site.

#### 3.2.1 Bump configurations

Wooden beams with two thickness (3,5 and 7 cm) were inserted into the bump experimental structure to create three geometric level crossing configurations (see Figure 14 and Figure 15 below) :

- configuration 1a: 0 cm,
- configuration 1b: 3,5 cm,
- configuration 1c: 7 cm.



**Figure 14.** Configuration 1 – Bump with wood beams

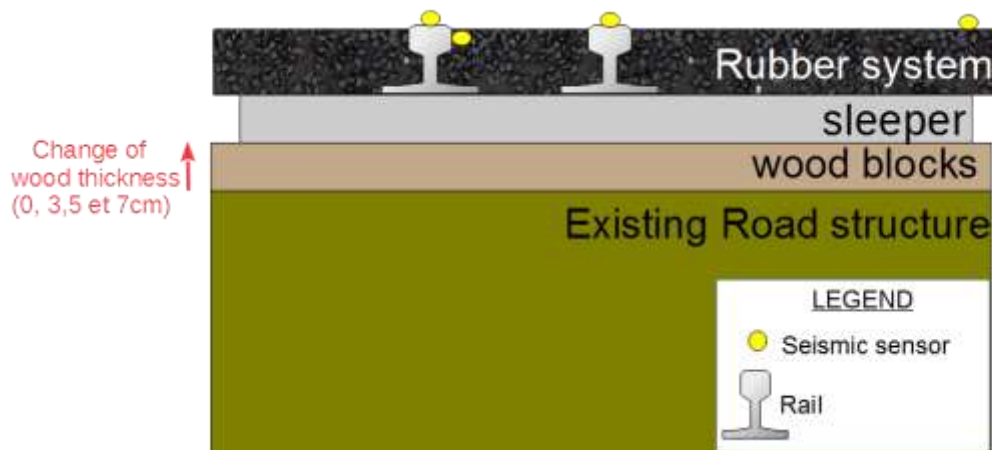


**Figure 15.** Bump experimental level crossing - two thickness of wood

For the bump configuration, photogrammetric and seismic measurements will be realized whereas the hollow configuration will be able in addition to that to make the thermo-infrared measurements featured by cracks.

### 3.2.2 Hollow configurations

The hollow configurations were made by using water-saturated sand inside waterproof film in combination with the passage of trucks to produce deterioration of the infrastructure (see Figure 16).





**Figure 16.** Configuration 2 – Hollow with saturated sand and truck traffic

The hollow configurations used in the piloting were:

- Configuration 2a': 0 cm, without truck passage
- Configuration 2b': 1,9 cm, after 1 truck passage – 3km/h
- Configuration 2c': 2,1 cm, after 1 truck passage – 12 km/h
- Configuration 2d' : 2,4 cm, after 1 truck passage – 12 km/h
- Configuration 2e': 2,8 cm. after 3 truck passages – 3 km/h, 3 truck passages – 12 km/h, 3 truck passages – 25 km/h, after 3 van passages – 15 km/h, 3 van passages – 25 km/h, 3 van passages – 30 km/h.

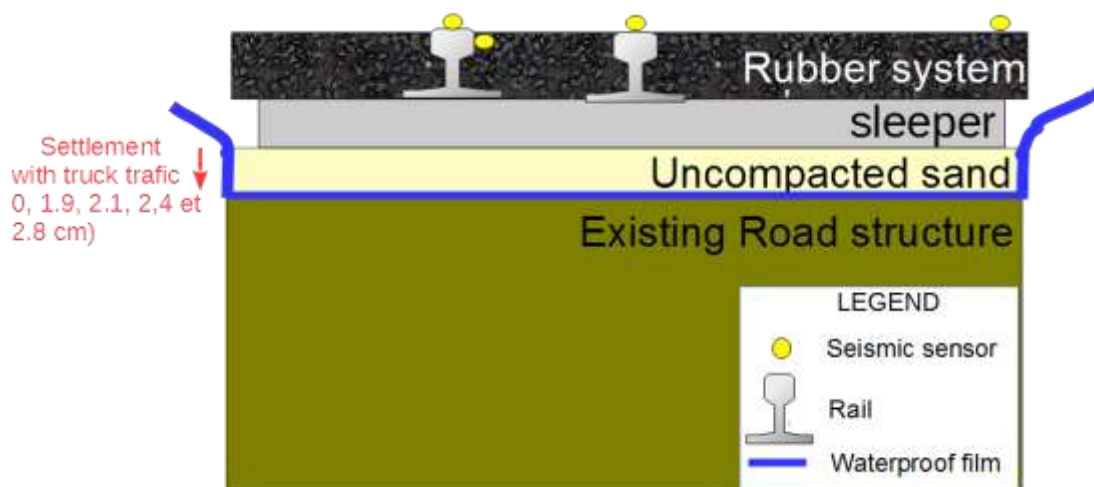


**Figure 17.** Hollow experimental LC – four steps with truck traffic

The different configurations (see Figure below) will be used to detect degradations of the level crossing.

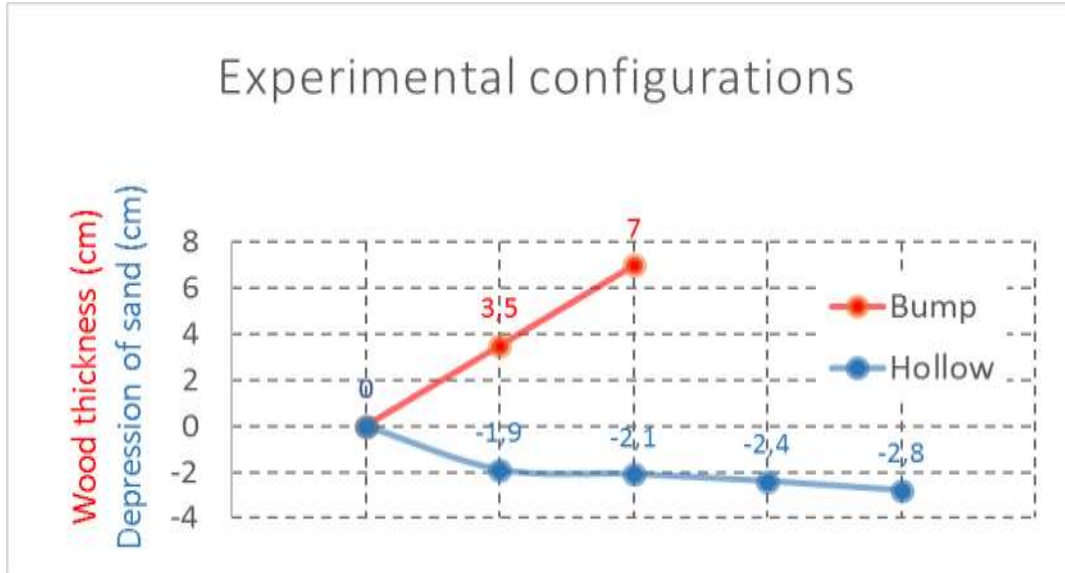


**Figure 18.** Geometry of the experimental configurations

The aim of this measure called as *Monitoring and remote maintenance* is to monitor the condition of LCs and detect potential problems with rail infrastructure (e.g. any deterioration) by using sensors on the track and road (seismic sensors, photogrammetric system and thermal infrared method). This measure aims to detect infrastructure conditions (and any deterioration of the structure) to avoid collisions at LCs between trains and heavy vehicles stuck at LCs. Railway managers already use topographic sections with a lower level of precision. The photogrammetric method will improve the detection of dangerous profiles.

Four methods will be tested as Table 1 bellow (see Figure 19 attachment):

**Table 1 :** Measurements used to detect surface degradations by configuration.

Configurations	Measurements
Bump 1a, 1b, 1c	Vibration, photogrammetry, VACC
Hollow 2a', 2b', 2c', 2d', 2e'	Vibration, photogrammetry, VACC, thermal infrared method

We added the VACC measurement (instrumented vehicle of Cerema) in the experimental plan.



Figure 19. Different methods tested on experimental LC test site.

### 3.3 Measurements used to detect surface degradations

The main aim is to test the different methods and to develop photogrammetric devices in real conditions. At first, an experimental structure of a rail panel with bump configuration is implemented, then with an hollow configuration characterized by saturating sand to distort faster under the truck passages (see Figure 15).

Four methods are tested on the experimental level crossing site : See the photos of the photogrammetry on Figure 20, seismic measure on Figure 28, thermo-infrared measure on Figure 29, and the instrumented vehicle of Cerema on Figure 30.

#### 3.3.1 Photogrammetric method

For the photogrammetry, the model was referenced with landmarks (see Figure 21). In total, eight photogrammetric references were used (Figure 21). Furthermore, a stabilizer was used on an instrumented ramp to keep horizontal movement stable. It compensates for tire suspension and stabilizes the movement of the camera ramp. Testing of the photogrammetric device was performed to set orientation and position of the cameras, and to identify the best speed have been carried out.



landmarks

**Figure 20 :** *Photogrammetric measure*

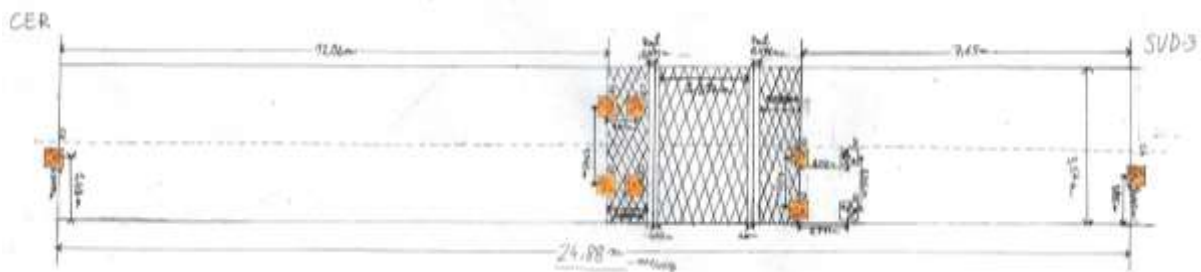


**Figure 21.** *Level crossing representation with photogrammetric references*

### 3.3.2 Vibration

Two loads were used for the seismic measurements: a truck (6,5t/wheel, a deflectograph) and a van (1,5t/wheel). Three different speeds were used for each vehicle type (see Table 3):

- Truck (6.5t/wheel): 3 km/h, 12 km/h and 25 km/h
- Van (1.5t/wheel): 15 km/h, 25 km/h and 30 km/h

The accelerometers and their position used in the test are presented in Figure 27. The location of the sensor placement is identified by using simple modelling of the structural dynamics of the LC. Standard commercial accelerometers with a range of 50g and uni-axis will be used at the CEREMA test site. Six sensors will be used in the same lane with two horizontal direction sensors and four vertical direction sensors.

A simplified model of the LC geometry and structure is developed and load cases with several axle loads passing have been analysed. The level crossing structure is composed of several layers of materials. The subgrade or the existing roadbed provides the foundation on which the various layers are placed. Figure 22 shown a cross section through the track and ground at for the test section. Figure 22 shown vertical axel loads from road and rail vehicle on the LC structure. Rail type of UIC60 on concrete sleeper at 600mm spacing was used.



The analysis is done for a vehicle wheel running over the LC with car speed ranging up to 60 km/h.



**Figure 22.** Cross section through level crossing.

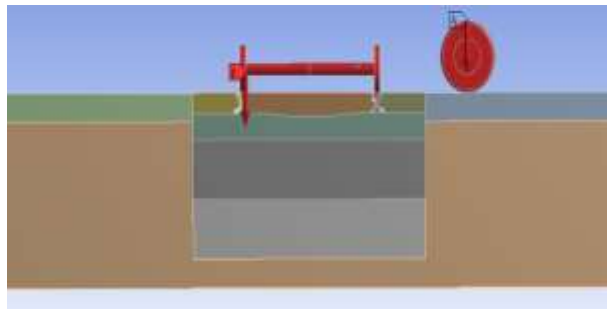


**Figure 23.** Axle loads from road vehicle and rail vehicle wheels.

A finite element model of the LC with all the different components are developed. The three-dimensional FE model is shown in Figure 24 consists of the rail, sleeper, ballast and sub ballast layer of soil. The physical dimensions and the material properties for the various layers is approximated to have the similar as the test site. The material parameters of the LC inner and outer part are listed in Table 2.

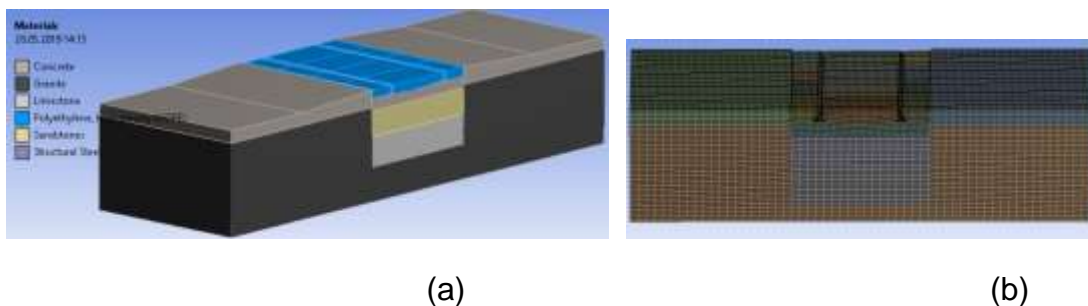


**Figure 24.** A simplified three-dimensional FE model of LC structures (a) and mesh of the model (b).

**Table 2 :** LC Rubber panel material parameter

Material	Dimension	weight
----------	-----------	--------

Rail gauge	1435 mm	
Inner element rubber	520mm X 172mm X 800mm	201,37 kg
Outer element rubber	1464mm X 198mm X 800mm	65,429 kg

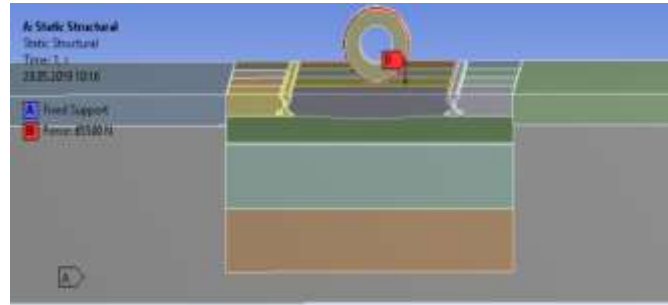


**Figure 25.** Vertical wheel load acting on the LC structure.

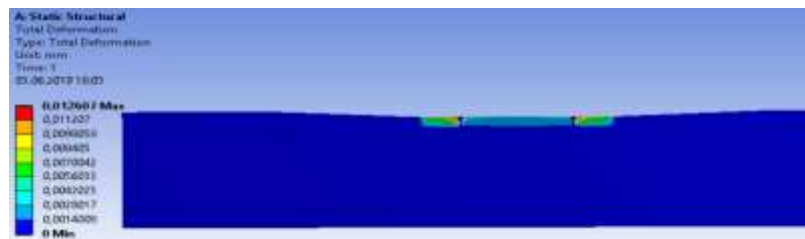
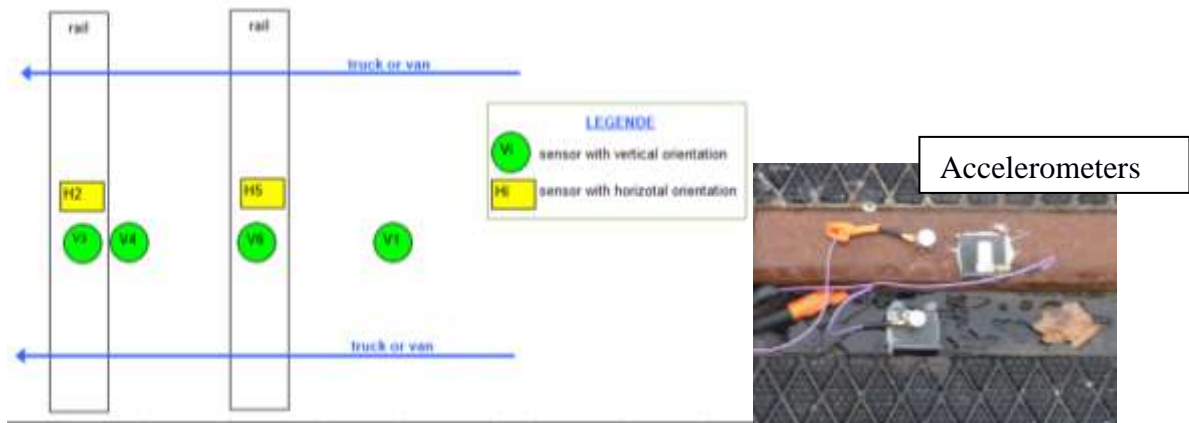


**Figure 26.** Vertical deformation due to wheel load running across the LC.

A wheel load acting on the level crossing is simulated in static and dynamic analysis, and the stress and deformation along the section is calculated, refer Figure 25. Flexible level crossing surface reflect the deformation of the lower layers on the surface. The maximum stress and deformation for different loading cases have been calculated, see Figure 26. Based on this simple modelling, the location for the sensor has been determined, as represented in Figure 27.



Name	Reference sensors	serial number	Measurement range (g)	Sensitivity (mV/g)
V1	PCB 321A02	978	± 50	99,2
H2	PCB 321A02	1055	± 50	100,3
V3	PCB 321A02	981	± 50	97,3
V4	PCB 321A02	980	± 50	97,8
H5	PCB 321A02	1060	± 50	97,1
V6	PCB 321A02	979	± 50	100,6

Figure 27. Accelerometers and their position.



Figure 28. Seismic measure.

Table 3 : Speed truck and van - seismic test.

Truck (6,5t/wheel) (km/h)	Van (1,5t/ wheel)
------------------------------	----------------------

	(km/h)
3	15
12	25
25	30

### 3.3.3 Thermoinfraréd

The collection of thermal infrared data required a high-resolution thermal imaging camera (FLIR Vue Pro 320\*240).



**Figure 29.** *Thermoinfraréd measurements.*

### 3.3.4 Equipped vehicle of Cerema (VACC)

The instrumented vehicle VACC (“Véhicule d’Analyse du Comportement des Conducteurs” in french) is a vehicle (Renault Mégane) that can record all the data passing through the A/D converter bus of the car; that is, data on the dynamics of the vehicle (used by the different safety devices) and the actions of the driver. This data is associated with video (front, back, steering wheel, pedals, driver) and GPS positioning.



**Figure 30** : VACC – Instrumented vehicle.

### 3.4 Scenarios used in the measurements

The different scenarios for configuration 1a, 1b, 1c, 2a', 2b' 2c', 2d' and 2e' are listed below:

- scenario 1: instrumented vehicle crossing the LC (moving at 8,5 km/h) for photogrammetric measure - moving forward
- scenario 2: loaded truck or van crossing the LC (speed 1) - moving backward
- scenario 3: loaded truck or van crossing the LC (speed 2) - moving backward
- scenario 4: loaded truck or van crossing the LC (speed 3) - moving backward
- scenario 5: instrumented vehicle crossing the LC (VACC)

A complementary scenario for configurations 2a', 2b', 2c', 2d' and 2e' is:

- scenario 6 : field HD thermal-infrared camera by pedestrian

For each configuration (1a to 1c and 2a' to 2e'), a levelling on rail was realised to compare photogrammetric results with full station measurement (see Figure 31). Four points (R1D, R1G, R2D et R2G) were realised in total and the result is the mean of these points (see

Table 4 and Table 5.



**Figure 31** : Rail leveling and reference measure of the full station.

**Table 4** : Levelling results of the bump configuration

Bump configuration		
Configuration	Thickness average (cm)	Std
1b	4.4	0.3
1c	8.9	1.0

**Table 5** : Levelling results of the hollow configuration

Hollow configuration		
Configuration	Thickness average (cm)	Std
2b'	1.9	0.5
2c'	2.1	0.8
2d'	2.4	0.8
2e'	2.8	0.6



## 4. DESCRIPTION OF THE PHOTOGRAMMETRIC METHOD

---

### 4.1 Choice of the photogrammetric method in the SAFER-LC project

In the context of developing an automatic method to follow a level crossing profile to perform the maintenance, Cerema proposed a system enable to give the surface state of a level crossing to have an acquisition of a 3D surface giving a surface distortion (see reference bibliography on photogrammetric methods [12], [13], and applications [14],[15],[16],[17],[18],[19],[20],[21],[22]).

Other techniques have been studied such as:

- Light Detection and Ranging (LiDaR), a pulse laser is sent to a surface, distance is computed using the reflected pulse with a sensor and knowing the speed of light,
- Structured light method.

These techniques have constraints, therefore the photogrammetric measurement has been chosen owing to the practical side and easiness of implementation. In the experimental zone, LiDAR is less easy to use for sweeping the whole zone, needing, for instance a drone. Structured light method has already been observed as another potential method to detect pavement cracks [23].





The principle is to collect data at different timestamps and compare the different data. The aim is to take into account distortion and analyse this profile to know if profile is dangerous.

### 4.2 Material description

A photogrammetric device was developed within the SAFER-LC Project to automatize the data capture and to have a 60% overlap between photos on equipped vehicle (see Figure 32 and see reference bibliography on device description [24],[25] and [26] with the help of Gaetan Curt, R&D Photogrammetry and Geomatics Engineer).

For the SAFER-LC project, photos of the level crossing had to be taken to differentiate between geometric profiles.

Legend :

-  : metal bar
-  : attachment point
-  : stabilizer DJI Ronin-MX
-  : Photo camera Sony Cyber-shot DSC-RX0 (in the cage port Sony VCT-CGR1)

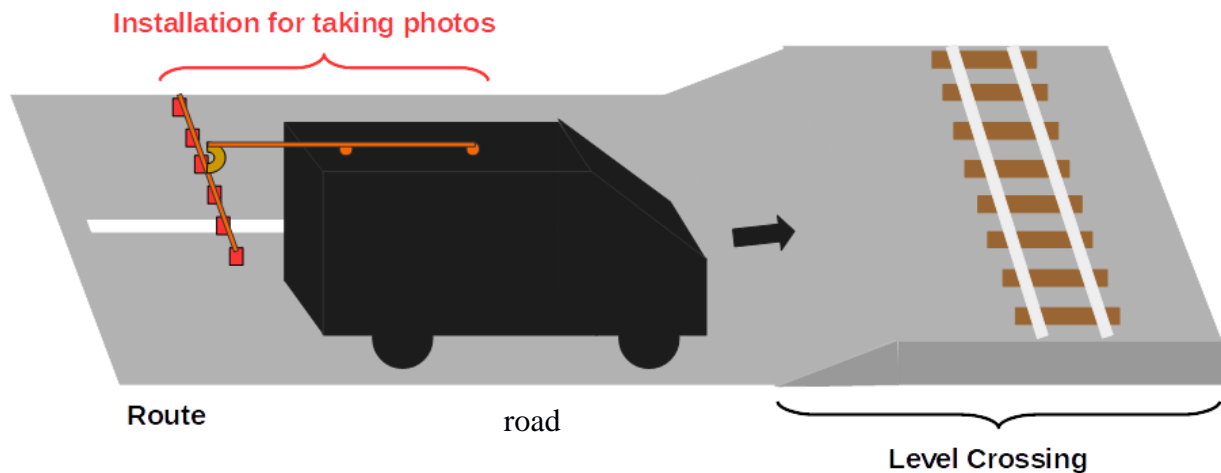




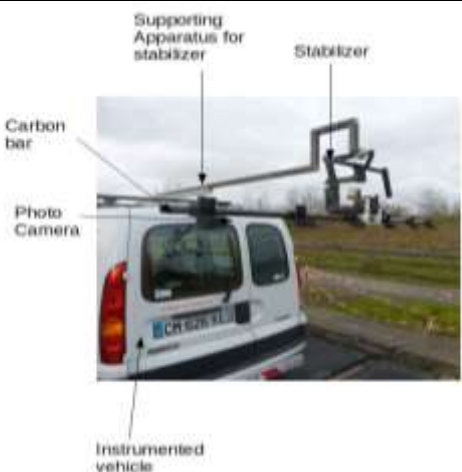
**Figure 32.** Device of the photogrammetric method.

Following all the requirements determined to get usable pictures, we made a carbon supportive bar to set the camera's position and orientation. We also made a supportive system to fasten the whole system on the roof of the vehicle. Stabilizer fixed on a supportive bar fixed on the roof of a van is used to decrease vibrations during video data collection.

Each camera has been installed on the carbon bar.

A support structure for photo cameras and stabilizer was built in the Experimental research centre and Studies and Prototype Design Centre (Cerema) for the project needs. For the stabilizer, a calibration and setting have to be done in order to ensure a parallel position of the camera to the ground.



Material		Features
Photo camera « Sony Cyber-shot DSC-RX0 » x6		Focal distance set at 8 mm 110 g /u Sensor 13,2x8,8mm 3.4 frames / s
Stabilizer « DJI Ronin-MX »		maximum load – bearing capacity of 4.5 kg
Supporting apparatus for stabilizer Carbon Supporting apparatus for photo cameras		

**Figure 33.** Equipped vehicle with the photogrammetric system.

Convergent view has been tested with the photogrammetric method developed. A quick test has been done to check if this configuration could be tested twice (in order to use the six cameras with two groups):

A group at the right of the stabilizer and the other one at the left (see Figure 34 below). Tests have been validated with an overlap photo slightly higher to 50% between the two groups.

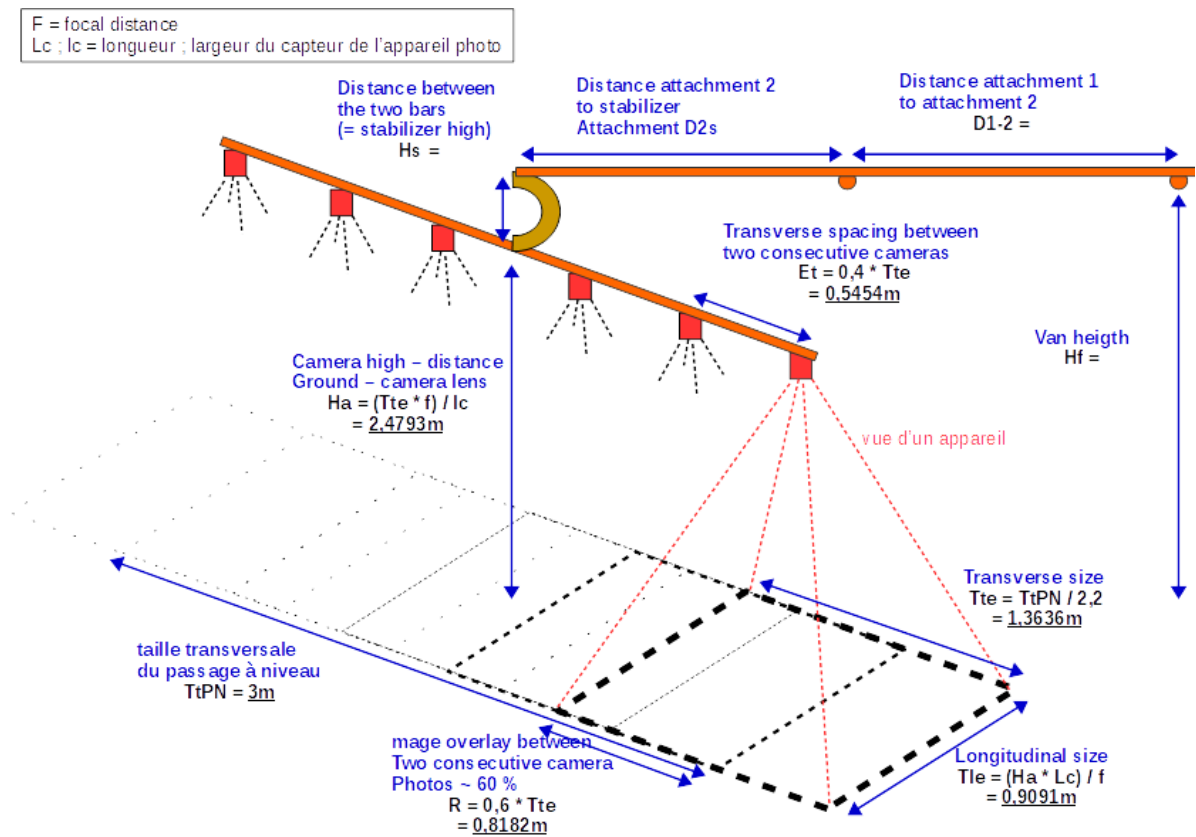


**Figure 34:** Details for the installation.

The rail panel is three meters wide; the photogrammetric system has to cover three meters of surface more. The van will have to cover to go and to return on the two tracks of the level crossing in order to covers six meters with 25% of overlaying photos, by ensuring that system covers 4.5 meter of surface. By exceeding by 0.75 meter from both side, photos of the first way overlap 1.5m, to go toward with 33% of the photos of return.

In order to cover a pavement width with a 60% overlap of photos, we concluded after various tests to use six cameras in two groups, each group being on each side of the stabilizer and converging on the scene corresponding to a width of three-meter road. This convergent view between the cameras gave good results. This arrangement of the camera was defined for the application of level crossings.

Focal distance of the camera is known (8 mm), photographic sensor size too (13.2 x 8.8 mm), and the height (Focal point – surface).

The height of cameras and the space between the cameras will be computed according to the following settings.

### 4.3 Settings definition

The geometrical parameters of the photogrammetric device has been calculated with the Gaussian approximation where a light ray passing through a thin, slightly open lens near the axis and is not deflected. In this configuration, the calculated theoretical resolution (smaller detectable detail) is 0.578 mm.

$$\begin{aligned} \text{Width of pixel} &= \text{Sensor width} / \text{Pixel number on the width} \\ &= 13,2 / 4800 \\ &= 0,0028 \text{ mm} \end{aligned}$$

$$\begin{aligned} \text{Resolution} &= (\text{pixel width} * \text{height}) / \text{focal distance} \\ &= (0.0028E-3 * 1.65) / 0.008 \\ &= 5.775E-4 \text{ m} \\ &= 0.578 \text{ mm} \end{aligned}$$

The theoretical resolution is widely sufficient (0.578 mm on road) for our application (to detect LC's deformations / cracks). To know the cover of a camera, gauss curve is used a light ray which crosses a thin lens not opened near the axle is not deviated.

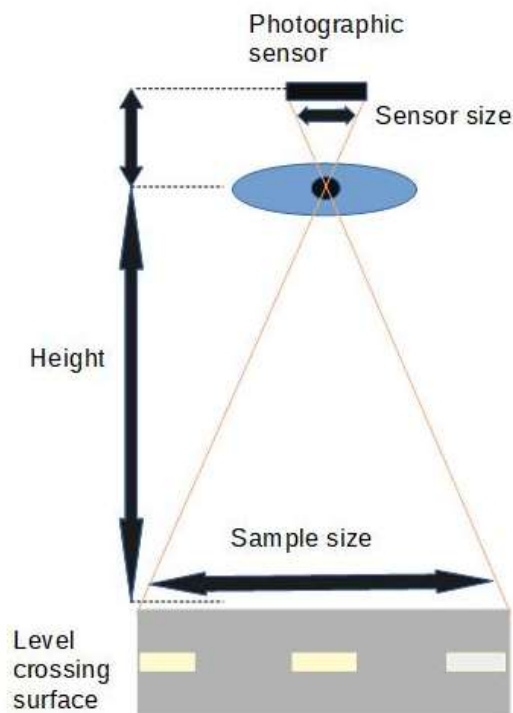


**Figure 35** : Approximation of a view from a photo camera (Gauss curve).

The van is two-meter-long, minus 35cm of the stabilizer: cameras will be suspended at 1.65m. With the Gauss curve, the size of the sample along its width can be computed by using the Thales theorem (see Figure 35).

Below are defined all variables of calculations

height = distance between camera and ground = 1.65 m

width sensor (of camera) = 0.0132 m

sensor length = 0.0088

Focal distance = 0.008 m

transverse sample = width covered by cameras 2 and 5 = 2.723 m

period of the frame capture = 0.294 s

#### Transverse sample size :

Transverse size = (height \* width sensor) / focal distance = 2.723 m

The six cameras are aligned, cameras 1,3, 4 and 6 can be disregarded (as they converge to view 2 and 5).

#### Spacing camera 2 and 5 :

Cameras 2 and 5 have to be perpendicular with the ground and covering a width of 2.72 m. They overlay each other at 60%.

Cameras have to be a spacing of 40% from the sample size so that:

Camera spacing 2 and 5 = 0.4 \* transverse sample = 1.089 m

#### Spacing cameras :

To simplify the installation, cameras need to have a spacing of the same gap :

Transverse spacing = (cameras spacing 2 and 5) / 3 = 0.363 m

#### Angle cameras 1, 3, 4 and 6 :

The angle and orientation for the cameras 1, 3, 4 and 6 will be oriented to converge to 2 and 5 so that :

- Tilt regarding to the ground = 90
- $\arctan(\text{height} / \text{transverse spacing}) = 12.41^\circ$

#### Longitudinal sample size :

All settings according to the width are done, and then settings according the length can be defined.

The previous layout can be used by taking into account the length of the sensor and not the width.

Longitudinal size of the sample = height \* sensor length / focal distance = 1.815 m

Longitudinal spacing :

Each consecutive photo taken with the movement of the vehicle covering 60% from the previous one, and as a consequence a shift of 40% of the sample length:

$$\text{Longitudinal spacing} = 0.4 * \text{longitudinal size of the sample} = 0.726 \text{ m}$$

Optimum vehicle speed :

After a test, cameras in the burst mode (continuous shooting) approximately takes 0.294 second.

$$\text{Optimum speed} = \text{longitudinal spacing} / \text{period of the capture} = 2.469 \text{ m/s} = 8.89 \text{ km/h}$$

Minimal attachment distance of the stabilizer :

Photos only have to show the ground surface. Attachment distance of the stabilizer is computed so that photos not cover the whole area behind the vehicle :

$$\text{Minimal attachment distance} = \text{longitudinal size of sample} / 2 = 0,908 \text{ m}$$

This distance is approximately set at 1 m to take into account cases for which vehicle get down a slope. (Cameras slightly shifts toward the vehicle).

## 4.4 Settings of the cameras

For all cameras, their settings have to be strictly identical owing to the following settings.

Camera settings	Explanations
« Quality » to « Extra fine »	To have computation more precise when doing data processing, the best and higher resolution is selected
« Shoot Mode » to « Manual Exposure »	Set the obstruction speed and the exposition time to have similar parameters.
« Shutter Speed » to « 1/1000 »	Shutter speed to 1/1000
« ISO » to « 200 » or « 400 » according to the light « AEL w/ shutter » to « Off » « White Balance » to « Daylight »	All settings are automatically set by default. Similar settings have to be set to compare photos.

« DRO/Auto HDR » to « Off »	
« Shoot Mode/Drive » on « Cont. Shooting »	Burst mode ( Shooting photos) as an automatic shooting photos mode.

Up to five photo cameras can be synchronized without any access point. Play memories application has a functionality to set all of them by using WIFI. An access WIFI point is needed to synchronize the six photo cameras. A router is then placed in the Van. After connecting the laptop, and all devices to the router, the test consist in placing them in front of the level crossing (10 meters approximately to have the profile before the level crossing), activating through the mobile the shooting photos, then crossing the level crossing when driving at 8-9 km/h, at the centre. Drive under 8 km/h is not a problem but takes more time for computing.

#### 4.5 Description of the photogrammetric data processing

During the first tests, the Photogrammetry-based method for LAndSlide Study and PLaS with photo scan software for treatment, was used. This method developed by Cerema Lyon for following the catchment basin movement and their progress uses photogrammetry in order to replicate surfaces at two different moments into a scatter plot then compare them (reference [15]). With this technique, surface displacements are measurable and quantify between the two moments. To follow the movement of a side mountain, the photos taken to the moment 1 (for example with configuration 1a) have to be compared with a set of the same photos taken at a moment 2 (for example with configuration 1b), and another moment. The conditions of sets making must be the same between moments 1 and another moment. It's important to calibrate indifferently each camera. With large photogrammetric models, it's necessary to use six cameras. First results led to deformed photogrammetric model with the same geometric deformation of each lens for a given type model of camera. Thus, it was necessary to consider own characteristics for each camera of the same type of camera. In this context, we use Micmac software with interface AperoDeDenis V5.48 (on github this software named "interface Cerema"), graphical user interface developed by Mr Jouin (Cerema).

This principle is used in the SAFER-LC project for the photogrammetric method to measure surface distortion. Each step is described in the following chart:

Step 1	Dense scatter plot
<b>Objectives</b>	Create different scatter plots relevant to set of photos of moment 1 and other moments <ul style="list-style-type: none"> <li>▪ Obtain the two scatter plots of moments 1 and another extension with the .txt extension</li> <li>▪ Compute the camera orientation and calibrate as MicMac software can analyse the location</li> <li>▪ Compare the different scatter plots with CloudCompare</li> </ul>

	<ul style="list-style-type: none"> <li>▪ Compute the displacements of corresponding points</li> <li>▪ Display on a graph result</li> <li>▪ Have the dense scatter plot</li> </ul>
<b>Environment</b>	<ul style="list-style-type: none"> <li>▪ MicMac</li> <li>▪ AperoDeDenis v5.48</li> </ul>
<b>Material used</b>	<ul style="list-style-type: none"> <li>▪ Photo cameras</li> <li>▪ Computers</li> <li>▪ Photogrammetric device</li> </ul>
<b>Operating mode</b>	<ul style="list-style-type: none"> <li>▪ The two scatter plots are created with the “.ply” extension</li> <li>▪ Necessary to scale different scatter plots with reference points</li> <li>▪ Superpose the two scatter plots to check their differences</li> <li>▪ Use the dense scatter plot and the non-dense scatter plot</li> <li>▪ Begin to sample the scatter plot with a number of digits defined by the user to reduce the compute time (for instance two digits for a centimetric accuracy)</li> <li>▪ Browse all (x,y) coordinates by checking for each point the difference between the z altitude of a point of the scatter plot 1 and the altitude z of the scatter plot 2</li> </ul>
<b>Step 2</b>	<b>Elevation difference between the models</b>
<b>Objectives</b>	<ul style="list-style-type: none"> <li>▪ Compare the different scatter plots</li> <li>▪ Compute the displacements of corresponding points</li> <li>▪ To analyse points with a defined abscissa and create a graph with <math>z = f(x,y)</math></li> <li>▪ To display on a graph the results</li> <li>▪ To have the dense scatter plot</li> </ul>
<b>Environment</b>	<ul style="list-style-type: none"> <li>▪ CloudCompare</li> </ul>
<b>Material used</b>	<ul style="list-style-type: none"> <li>▪ Photo cameras</li> <li>▪ Computers</li> <li>▪ Photogrammetric device</li> </ul>
<b>Operating mode</b>	<ul style="list-style-type: none"> <li>▪ The two scatter plots are created with the “.ply” extension</li> <li>▪ Necessary to scale different scatter plots with reference points</li> <li>▪ Superposed the two scatter plots to check their differences</li> </ul>
<b>Step 3</b>	<b>Test profile function</b>
<b>Objectives</b>	<ul style="list-style-type: none"> <li>▪ To obtain the geometric profile of the level crossing</li> </ul>
<b>Environment</b>	<ul style="list-style-type: none"> <li>▪ Python</li> <li>▪ MicMac</li> <li>▪ AperoDeDenis v5.48</li> </ul>
<b>Operating mode</b>	<ul style="list-style-type: none"> <li>▪ To obtain the profile of the level crossing, the user can fill in the data of the vehicle</li> <li>▪ The features of the vehicle are <ul style="list-style-type: none"> <li>○ size of the vehicle, spacing between wheels front, rear or holder false and tire contact surface</li> <li>○ -its ground clearance</li> </ul> </li> <li>▪ According to all settings of the vehicle, the test profile function checks for each ground point if with these features, the vehicle can scratch the surface</li> <li>▪ The points of this zone considerate dangerous and enhances in a result graph</li> </ul>



## 5. DESCRIPTION OF THE VIBRATION MEASUREMENT METHOD

---

Another important aspect in safety of LCs is the deterioration grade of the infrastructure, which can be correlated with an unexpected dynamic behaviour of road vehicles crossing the inter-section; in severe cases, a complete arrest of the vehicles might occur. Monitoring of the gradual wearing of the infrastructure, and its subsequent maintenance, is therefore desirable.

Two efficient and cost-effective solutions have been developed to this end. The first makes use of direct detection of the infrastructure geometrical profile through a photogrammetry method, i.e. reconstructing the three-dimensional coordinates of the infrastructure's surfaces points through photographs. The second method consists in the correlation of the wear grade of the infrastructure with the acceleration levels obtained through the employment of several accelerometers displaced in the operating infrastructure. The latter method is particularly appealing for its cost-effectiveness and the reliability of the acceleration data. The present study focuses on the development of efficient and cost-effective monitoring systems of the wearing level of LCs through the deployment of accelerometers.

### 5.1 Vibration measurement

Infrastructure Managers want to support the level crossing inspection with seamless data management and remote inspection. In this project, the use of smart and embedded wireless sensor networks to gather accurate information about the condition of LC was investigated originally. The idea behind the measurement system were to install wireless vibration sensors on the relevant track/road components and to collect data which will be transmitted with an alert threshold to the relevant bodies to inform the status of the LC components. Further, in case of major faults, malfunctions or damages that may have safety risk for the LC users, the system will enable to send alerts to LC users, track infrastructure managers, train operators, road traffic managers, etc, to prevent the user of possible safety risks due to the infrastructure deformation. The data exchanging and data sharing part is planned to be coupled to Task 3.4.

Wireless sensor networks (WSN) have been developed for different applications. Lee et.al [27] used wireless accelerometer sensor modul with 2-axis accelerometer sensor to detect activity and fall. The architecture of WSN is designed for continuous and real-time monitoring using distributed wireless sensors and the application areas of such WSN are very broad. Recently wireless sensors have been used for condition-based maintenance (CBM) in different engineering systems where it is difficult or impossible to use wired system. A WSN was applied for machinery condition-based maintenance (CBM) in small machinery spaces using commercially available products [28]. A single-hop sensor network was implemented to facilitate real-time monitoring and extensive data processing for machine monitoring.

However, due to several difficulties in terms of professional expertise, the implementation of WSN has been dropped and commercially available wired vibration sensors has been used



and installed in the test site. The vibration measured data is collected and a method has been developed to set different levels. The vibration levels for a normal operation of the LC has been categorised in several thresholds for predictive maintenance applications.

## 5.2 Accelerometers data processing

The processing of the data extracted from the accelerometers employed in the operating level-crossing can follow standard processing for vibration diagnostics. Vibration diagnostics is commonly employed for the maintenance of machinery, usually rotating components. The term diagnostics is usually used for monitoring and evaluating the condition of a machine during operation [29]. Vibration diagnostics involves information about the cause of vibration and detection of developing a fault. This method is especially suitable for the diagnostic of rotating machinery, where vibrations at particular frequencies are readily associated with well-known wear dynamics. However, the same procedure can be employed for the general assessment of the vibration levels of operative machinery and/or infrastructure.

The most common way to analyze vibration is in the frequency domain. Frequency analysis is performed by Fourier transform (by its decomposition into Fourier series) [29].

A classical definition of the Fourier transform is the following:

$$f(\xi) = \int_{-\infty}^{\infty} f(x) e^{-2\pi i x \xi} dx \quad (5.1)$$

where  $x \in \mathbf{R}$  and  $\xi \in \mathbf{C}$ . If  $x$  is measured in seconds,  $\xi$  should be in cycles per second for the formula to be valid. Then, either  $\xi$  must be in the so-called angular frequency, i.e.,  $2\pi f$ , or one must insert some constant scale factor into the formula. Thus, in the time domain:

$$f(2\pi f) = \int_{-\infty}^{\infty} f(t) e^{-i\omega t} dt \quad (5.2)$$

An algorithm called Fast Fourier Transform (FFT) is used in up to date analyses. Since the algorithm is based on the discretization of the FT, one should take care of related issues, such as aliasing and leakage errors [29].

Figure 36 shows an example of DFT of a quasi-periodic time domain signal. A common way of evaluating spectra in practice considers at first the measurement of the reference (baseline) spectra in all the measurement points when the machine or infrastructure is in a good state. Then, the same points are measured at different states, and the measured spectra are compared to the baseline spectra to detect relevant trends and wear information [29].

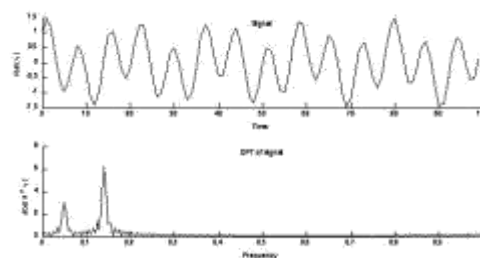


**Figure 36:** DFT time domain example.

Table 6 shows the main frequency domain analysis techniques for acceleration data [30]. The power spectral density is computed directly from the Fourier transform of a time series. The PSD describes the distribution of power into frequency components composing that signal [31]. In the general case, the units of PSD will be the ratio of units of variance per unit of frequency.

By defining a truncated Fourier transform where the signal is integrated only over a finite interval  $[0, T]$ , one can get the so-called amplitude spectral density:

$$f(2\pi f) = \frac{1}{\sqrt{T}} \int_0^T f(t) e^{-i\omega t} dt \quad (5.3)$$

Then the power spectral density, PSD, can be defined as:

$$S_{xx}(2\pi f) = \lim_{T \rightarrow \infty} \mathbf{E} \left[ |f(2\pi f)|^2 \right] \quad (5.3)$$

where  $\mathbf{E}$  denotes the expected value [32].

**Table 6 : Frequency Domain Analysis Techniques [30]**

Analysis Technique	Units	Use
Power Spectral Density	$[g^2 / \text{Hz}]$	Estimate of distribution of energy with respect to frequency
Cumulative RMS Acceleration	$[g_{rms}]$	Quantifies contributions of spectral components to overall RMS acceleration level for time period
RMS Acceleration	$[g_{rms}]$	Quantifies contributions of spectral components per frequency bin
Spectrogram	$[g^2 / \text{Hz}]$	Road map of how acceleration signals vary with respect to both time and frequency

### 5.3 Alert threshold levels definition

Standard ISO 10816 provides guidance for the assessment of machine condition for different types of machines based on two criteria [29]:

- Vibration magnitude;
- Change in vibration magnitude.

In the case of measurement of the vibration magnitude, the standard defines the highest value of vibration measurement at different locations as vibration severity. The standard

defines evaluation limits of the vibration severity. Based on these limits, a machine can be classified according to its state into one of four zones [29]:

- Zone A - Vibration of newly commissioned machines;
- Zone B - Machines with vibration within this zone are normally considered acceptable for unrestricted long-time operation;
- Zone C - Machines with vibration within this zone are normally considered unsatisfactory for long-term continuous operation (Warning Level);
- Zone D - Vibration values within this zone are normally considered to be of sufficient severity to cause damage to the machine;

Classification of the machine into one of the zones would help to decide about the future operation of the machine and to propose necessary action (shutdown, repair, etc.).

Following the guides given by the standard as a reference, it follows that, in the case of operation of an LC infrastructure, it is sufficient to define three zones, i.e., a reference zone, a warning zone, and a danger zone. Zone limits are indicative values rather than strict ones and may be adjusted.

The photogrammetric method defines situations of discrete physical profiles or status of the physical features of the LC surface in relation to the physical dimensions of the passing cars. These data are extracted from the photogrammetric measurements and levels of dangerousness of the different physical levels are set. By using these levels, the three zones are defined.

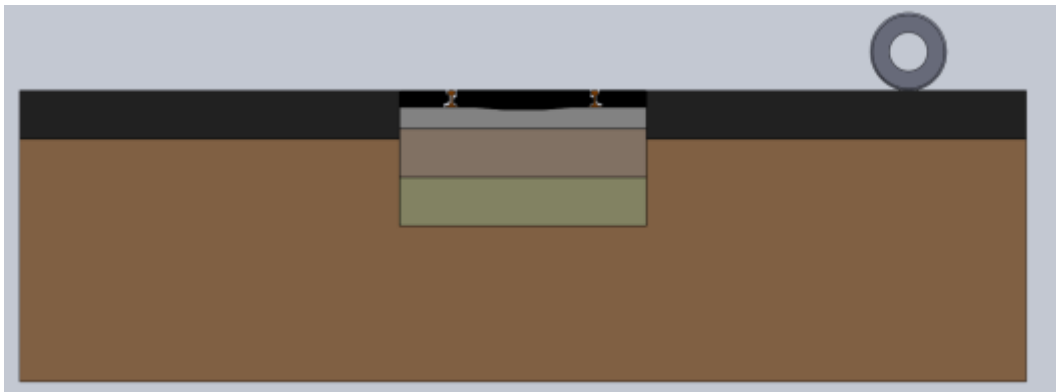
### **5.3.1 Warning and Danger levels for a LC**

Field vibration measurements are needed for the definition and calibration of the zone limits for the LC infrastructure. The number of relevant parameters needed during the tests has to be adequate in order to correctly define standard and danger limits and, through a parameter trend analysis, a warning limit.

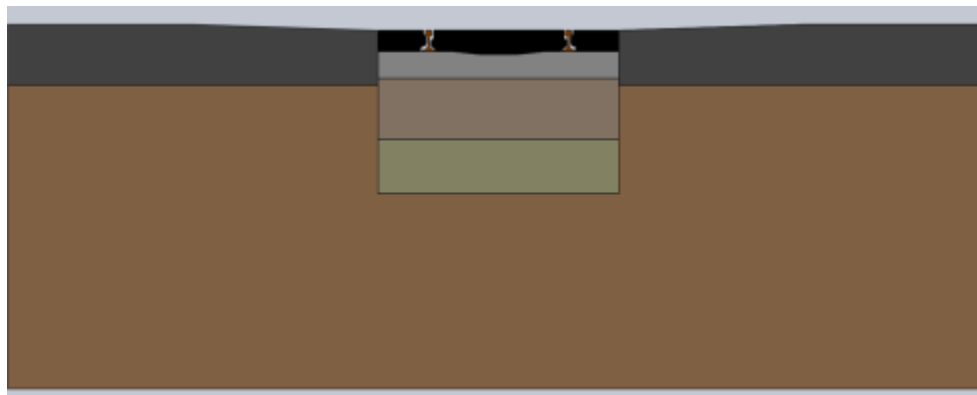
Table 7 shows the parameters varying during the measurements campaign. The deployment of a specific system for varying the relative height between rail and road during the measurements campaign makes possible to simulate different wear levels of the LC. The equivalent wear situations are represented by the parameter "configuration". Figure 37 shows the LC vertical profile configurations: standard, hollow and bump. In the experimental work, several levels of bumps and hollows have been used and vibration data of the respective levels are collected. A total of six accelerometers are used for data acquisition, distributed along with the infrastructure. The standard level is defined by considering a normal dynamic condition of the infrastructure; the danger level is defined by considering the most loaded dynamic condition of the infrastructure; the definition of a warning level, finally, is only possible after a proper trend analysis specific to the considered infrastructure.

**Table 7 : Analysis factors**

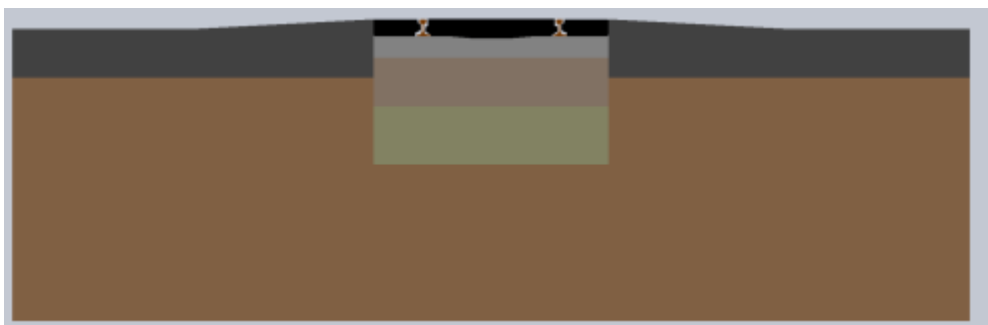
Factor		+		-
Vehicle type, $V_e$	[-]	$V_{e_{heavy}}$		$V_{e_{light}}$
Vehicle speed, $V$	[Km/h]	$V_{high}$	$V_{st}$	$V_{low}$
Configuration, $Conf$	[-]	<i>bump</i>	<i>standard</i>	<i>hollow</i>



a) Reference condition with no vertical profile variation between the LC and the approaching roadside.



b) Representation of sagging or hollow LC configuration



c) Representation of bumpy LC configuration

**Figure 37:** Different vertical configuration of LC profile a) standard, b) hollow and c) bump.

A PSD is computed for each accelerometer signal. For each dynamic situation, the RMS information and the peak value of the PSD of each accelerometer channel are used to define the dynamic situation's equivalent vibration severity level.

Generally speaking, the analysis dynamic situations can be defined in the following manner:

- Reference
  - Standard [ $V_{st}$ ;  $Ve_{light}$ ; *standard*]
  - Danger [ $V_{high}$ ;  $Ve_{heavy}$ ; *bump*]
- Trends
  - Configuration trend
    - [ $V_{st}$ ;  $Ve_{light}$ ; *bump*]
    - [ $V_{st}$ ;  $Ve_{light}$ ; *hollow*]
  - Dynamic trend
    - [ $V_{low}$ ;  $Ve_{light}$ ; *standard*]
    - [ $V_{high}$ ;  $Ve_{heavy}$ ; *standard*]

where two reference levels are defined, i.e., a standard and a danger level. The danger level is related to the most dynamically loaded case, and it is affected by both dynamic loads (vehicle mass, vehicle speed) and generalized wear loads (bump-hollow configuration). The trend levels consider single dynamic and configuration variations.

## 5.4 Data analysis

The data gathered during the experimental campaign are lacking the variation of the parameter previously defined as configuration. The collection includes data related only with the variation of vehicle speed and vehicle type. Therefore, it is possible to process only a limited amount of information regarding the dynamic trend of the LC infrastructure. In order to define an equivalent warning-danger level, the "heavy" case in the dynamic trend will be considered as the most loaded case in the analysis.

### 5.4.1 Vibration data in time domain

Two examples of the raw data collected during the experimental campaign are shown in Figure 44 and Figure 39. Three signals are associated with each accelerometer channel. Only the signal with the fairly best quality is considered in the analysis process. Some of the data are characterized by remarkably high noise peaks. The signals selected are depicted in Table 7.

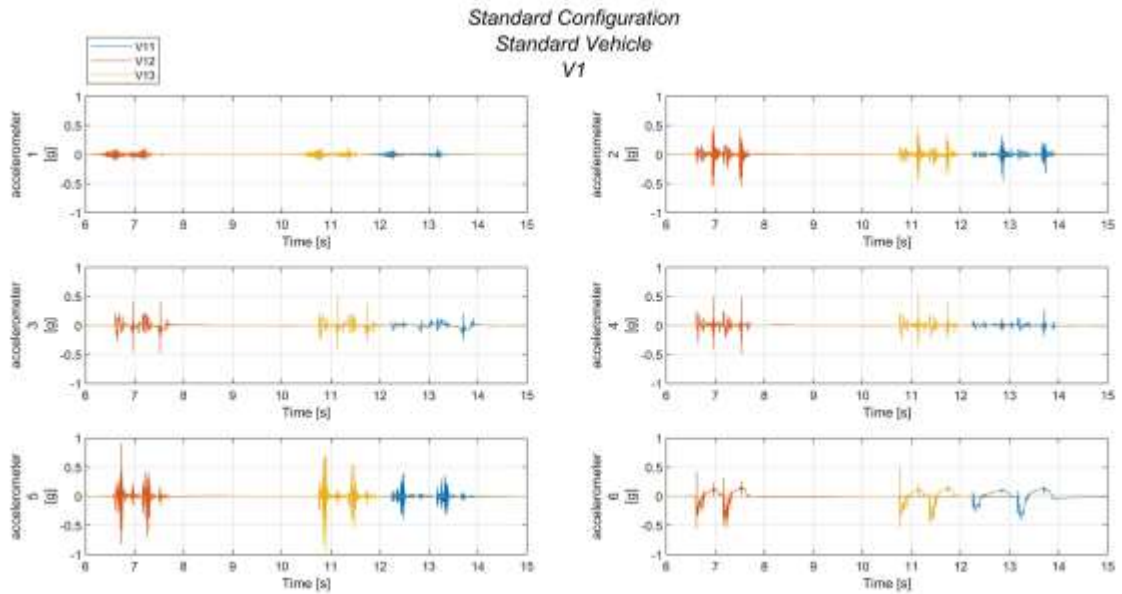


**Figure 38:** *Vibration data in time domain. Case: [Standard Conf, Light vehicle  $V_{light}$ , Low vehicle speed  $V_{low}$ ]*

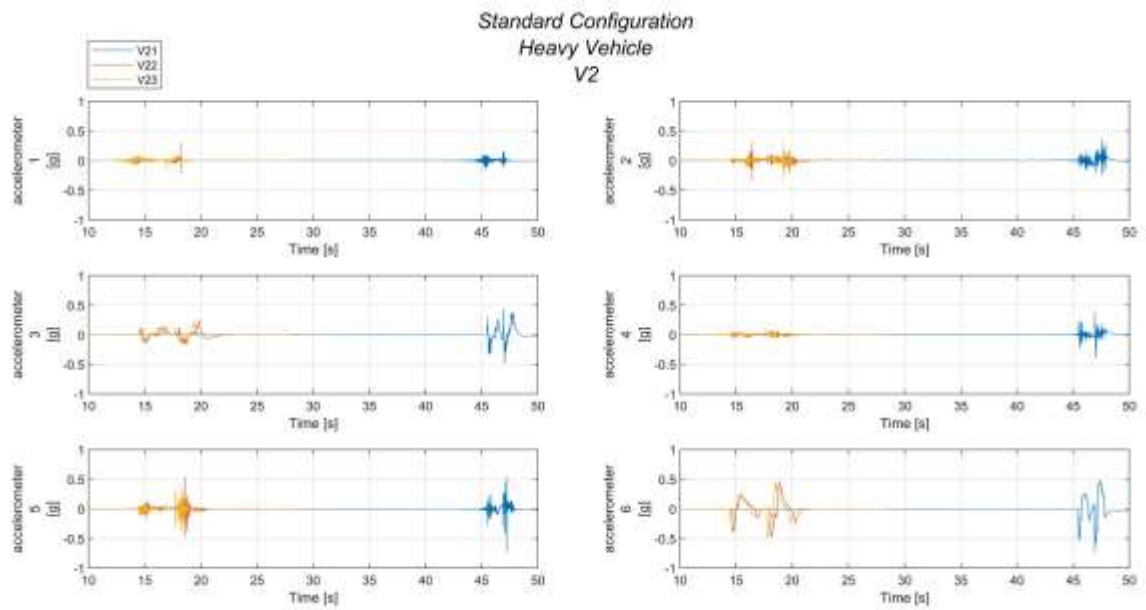


**Figure 39:** *Vibration data in time domain. Case: [Standard Conf, Heavy vehicle  $V_{heavy}$ , Standard vehicle speed  $V_{standard}$ ]*

**Table 8 :** *Signals selected*

Dynamic situation	Signal selected
-------------------	-----------------



Standard, Standard Vehicle, V low	Signal 1
Standard, Standard Vehicle, V standard	Signal 3
Standard, Standard Vehicle, V high	Signal 3
Standard, Heavy Vehicle, V low	Signal 2
Standard, Heavy Vehicle, V standard	Signal 3
Standard, Heavy Vehicle, V high	Signal 2

### 5.4.2 PSD analysis

The PSD data extracted from the time domain signals are shown in Figure 40 -Figure 45. The PSD has been estimated by using the Welch's overlapped segment averaging estimator. Accelerometer channels 1, 2, and 5 are detecting vibratory resonances at different frequencies: accelerometer 1 at about 1100 Hz, accelerometer 2 at about 900 Hz, and accelerometer 5 at about 1400 Hz.

With respect to the dynamic cases previously defined,

Figure 41 shows the PSD associated with the Reference-Standard case; Figure 45 shows the PSD associated with the Dynamic Trend - Heavy case; Figure 40 can be finally associated with the Dynamic Trend - Light case.

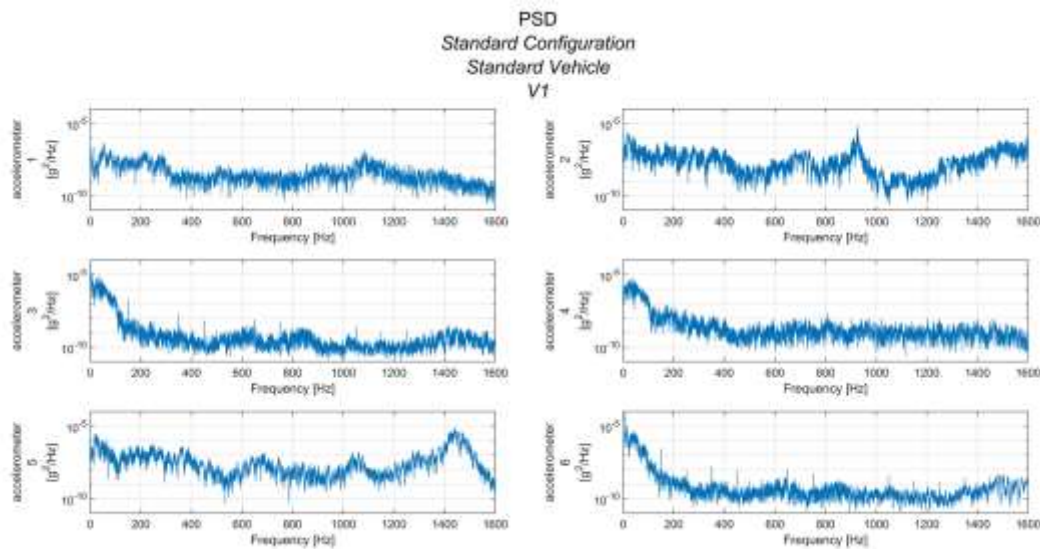


**Figure 40:** PSD. Case: [Standard Conf, Light vehicle  $V_{light}$ , Low vehicle speed  $V_{low}$ ]

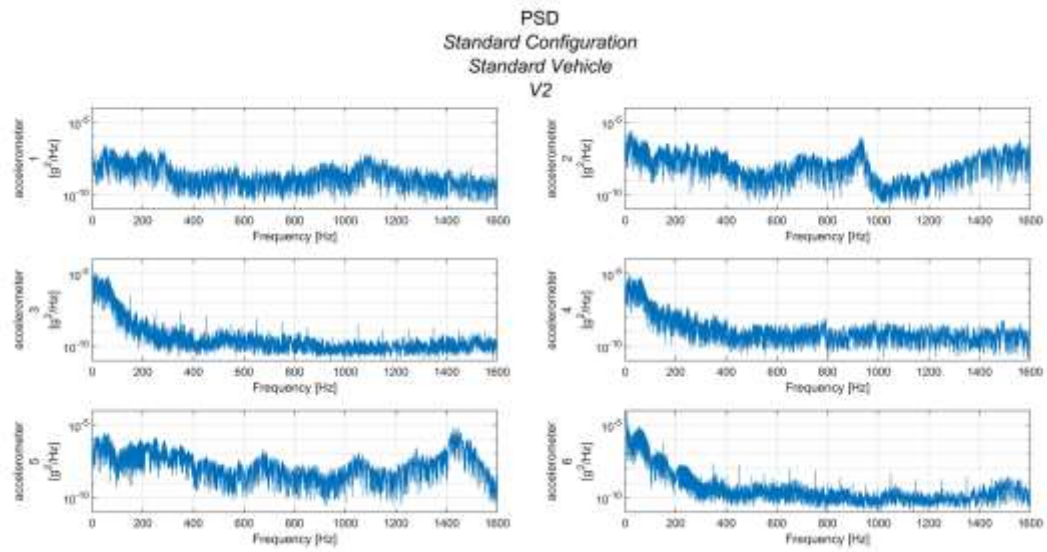


Figure 41: PSD. Case: [Standard Conf, Light vehicle  $V_{light}$ , Standard vehicle speed  $V_{standard}$ ]

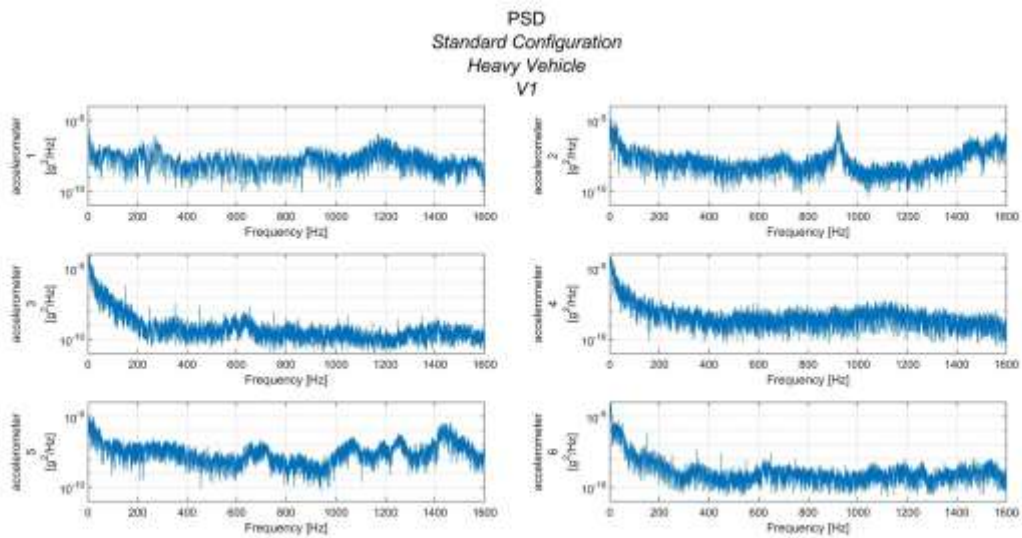
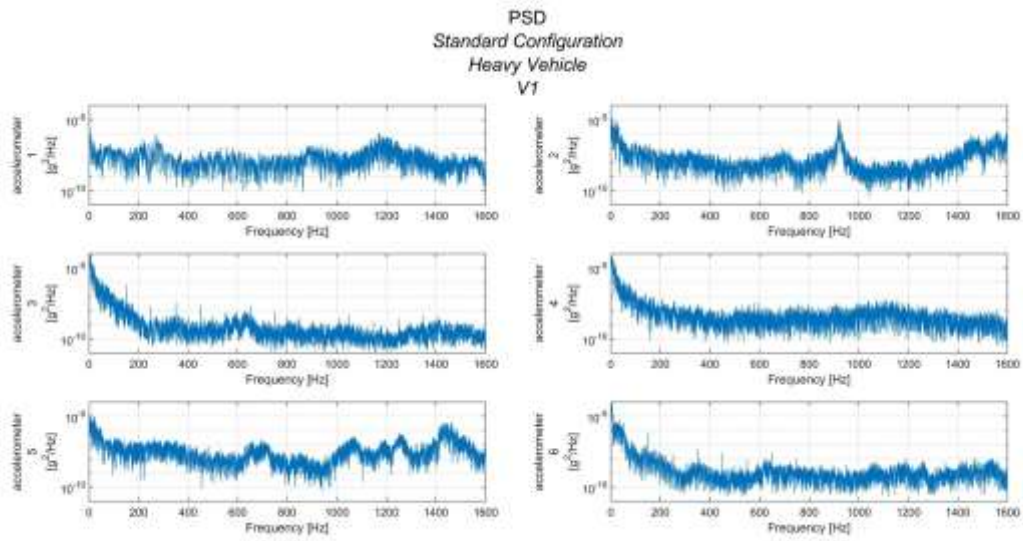
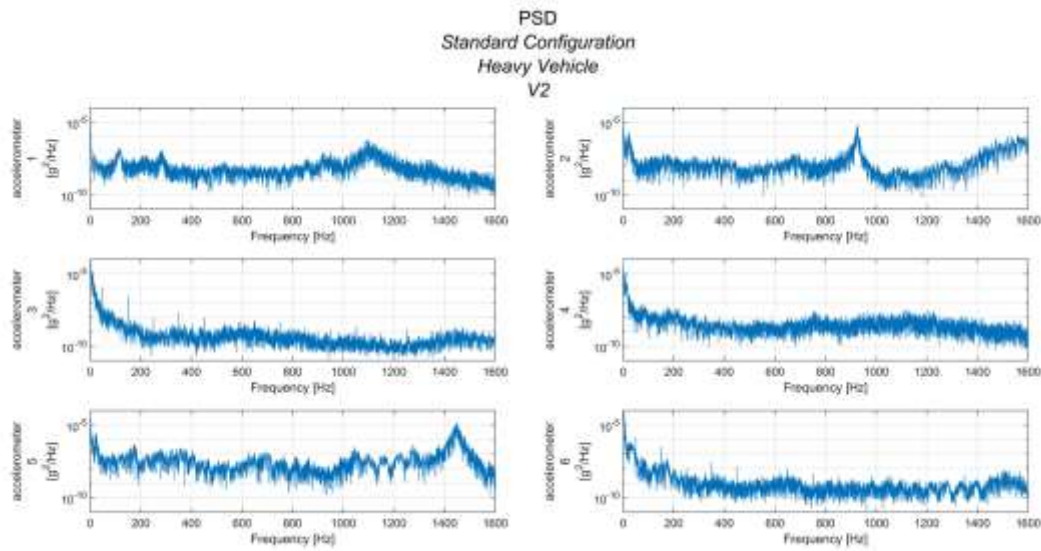


Figure 42: PSD. Case: [Standard Conf, Light vehicle  $V_{light}$ , High vehicle speed  $V_{high}$ ]



**Figure 43:** PSD. Case: [Standard Conf, Heavy vehicle  $V_{heavy}$ , Low vehicle speed  $V_{low}$ ]



**Figure 44:** PSD. Case: [Standard Conf, Heavy vehicle  $V_{heavy}$ , Standard vehicle speed  $V_{standard}$ ]

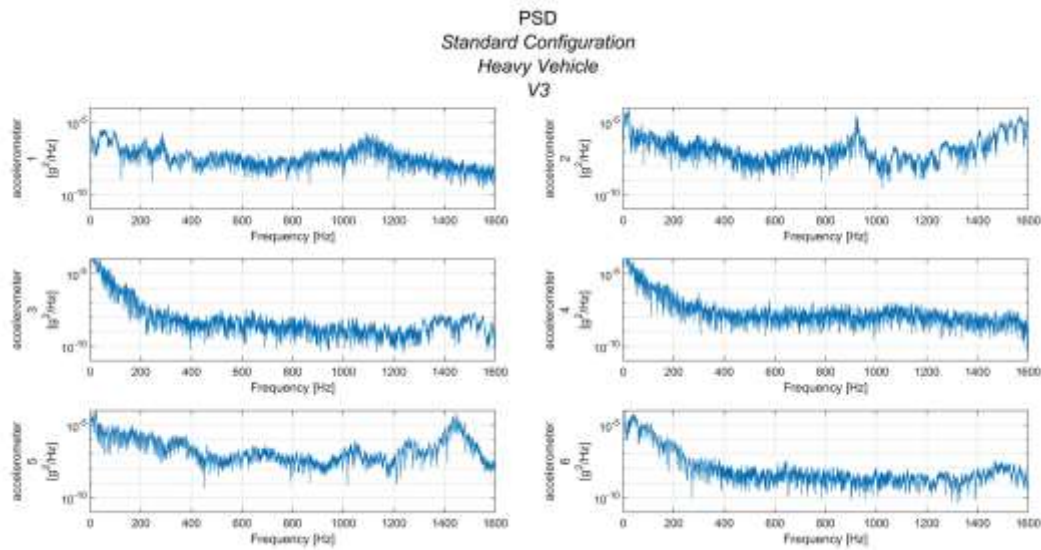


**Figure 45:** PSD. Case: [Standard Conf, Heavy vehicle  $V_{heavy}$ , High vehicle speed  $V_{high}$ ]

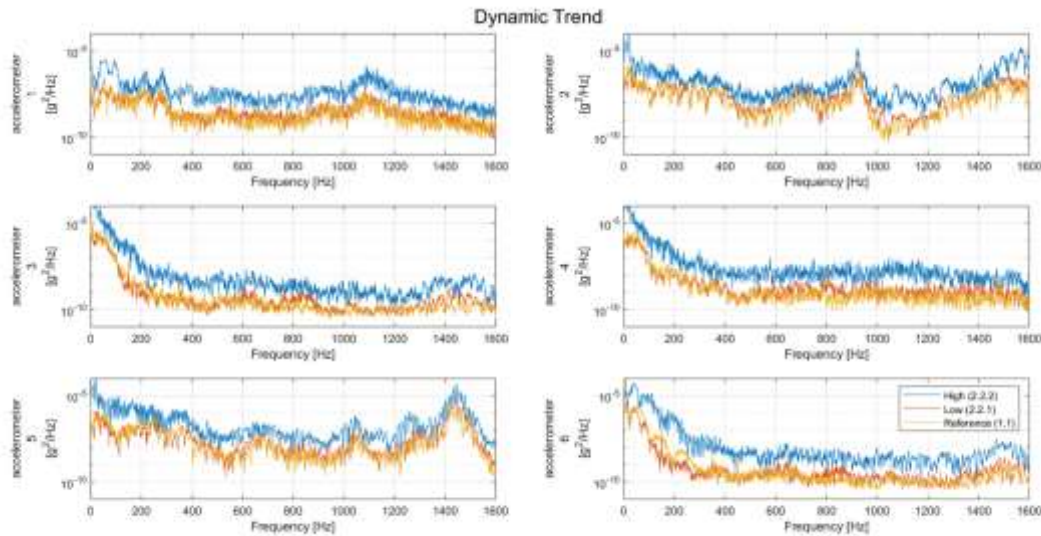


**Figure 46:** Dynamic trend - PSD variation

Figure 46 shows the dynamic trend in terms of the variation of PSD signals for each accelerometer channel. The Welch's PSD estimation window is composed of 4000 segments. No clear distinction can be qualitatively detected between the standard case and the case at low speed; however, a significant over-all increase of the PSD response is visible for the case at high speed and heavy vehicle.

Table 9 shows the computed RMS and PSD peak values. The RMS values have been computed in the lapse of time in which the absolute value of the acceleration signal returned a higher value than a predefined tolerance, 0.01 g. Accelerometer 6 is the most loaded for

every dynamic situation. The values related with the most dynamically loaded case, i.e., the "dynamic trend - heavy" case, can be used as a basis for the definition of an equivalent threshold warning level.

**Table 9 : RMS and PSD peak levels - Vibration Analysis**

Dynamic situation	Accelerometer	RMS [ $g_{rms}$ ]	PSD peak [ $g^2/Hz$ ]
Standard, Standard Vehicle, V low (DYNAMIC TREND - LIGHT)	1	0.011	2.2e-6
	2	0.0323	2.2e-5
	3	0.0404	1.08e-4
	4	0.0271	1.07e-5
	5	0.0461	7.9e-6
	6	0.1065	1.4e-3
Standard, Standard Vehicle, V standard (STANDARD)	1	0.0115	3.88e-6
	2	0.0307	3.2e-5
	3	0.0453	4.54e-5
	4	0.0356	8.22e-6
	5	0.0476	6.72e-6
	6	0.1163	1.2e-3
Standard, Standard Vehicle, V high	1	0.0197	1.73e-6
	2	0.0517	1.77e-5
	3	0.0690	2.42e-5
	4	0.0642	4.52e-5
	5	0.0846	1.67e-5
	6	0.1074	7.66e-4
Standard, Heavy Vehicle, V low	1	0.0293	11.18e-5
	2	0.0565	1.47e-4
	3	0.1458	2e-3
	4	0.0685	6.8e-5
	5	0.0617	3.7e-4
	6	0.2131	4.7e-3
Standard, Heavy Vehicle, V standard	1	0.0122	2.7e-5
	2	0.0217	1.32e-4
	3	0.0678	3e-3
	4	0.0171	1e-4
	5	0.0337	1.66e-4
	6	0.1594	1.2e-3



Standard, Heavy Vehicle, V	1	0.0391	2.65e-5
high (DYNAMIC TREND -	2	0.1144	4.38e-4
HEAVY)	3	0.199	2.1e-3
	4	0.1705	6.15e-4
	5	0.1348	7.74e-4
	6	0.2827	7.6e-3



## 6. LC BARRIER AND TRAFFIC LIGHT MONITORING METHOD

---

Level crossing has either active protection or passive protection. So far as warning systems for road users are concerned, level crossings either have passive protection, in the form of various types of warning signs, or active protection, using automatic warning devices such as flashing lights, warning sounds, and barriers or gates. Train traffic has priority at all time, so the road traffic must wait an approaching train. In Europa, about half of the LCs are active level crossing. Active protected level crossing considers any type of protection, which change its state (sound, light or mechanical) according to the approaching train. In most of European railways, automatic level crossing protection uses flashing light and sound traffic sign or it uses half barriers with the sound and flashing light. The normal functioning of these active control system is important for a safe crossing of other LC users and to avoid any collision with the incoming train. The active system informs users to use the road and to cross safely or to stay on the approach road before entering to the LC area. The electronic warning devices used are also referred to as grade crossing signals. Modern radar sensor systems can detect if level crossings are free of obstructions as trains approach, and improving safety by not lowering crossing barriers that may trap vehicles or pedestrians on the tracks while signalling trains to brake until the obstruction clears [33].

### 6.1 Automatic control system

Major components of active control systems used automation by use of sensors, such as vibration sensors and IR sensors. Barrier gates opening and closing is automatic as a train approaches the railway crossing from either side. Sensor placed at a certain distance from the gate detects the approaching train and accordingly control the operation of the gate.

A full barrier is a type of barrier gates where lifting of barriers on both sides of the road to protect the LC entry. Road traffic lights and an audible (sound) warning are also commonly provided. The barriers are normally kept in the raised position and, when lowered, extend across the whole width of the road carriageway on each approach, see Figure 47. Just before the boom are lowered, red flashing signals are lighted against road traffic.



**Figure 47:** Level crossing with light signal and full-boom.

There are also half-barrier boom systems together with road traffic light signals and sound warnings, see Figure 48. A lifting barrier on both sides of the road protect this type of crossing. Lifting barriers normally kept in the raised position and pivoted on the right hand-side of the road. When lowered, the barriers only extend across the entrances to the crossing leaving the exits clear. The half booms block road traffic from the incoming driving direction so that the road users can drive unobstructed on the other side if they have entered the level crossing towards red signal.



**Figure 48:** Level crossing with light signal and half-boom.

Level crossing may sometimes be equipped only with light and sound signals, see Figure 49. The warning light usually controlled by the nearest block track fields. When the track block fields are free, light shows only warning light. If the road signal is not in normal operation, a road signal should show red light. An audial signal should be placed to the right of the road, normally on the road signal. Several audio signal can be set up so that all roads are covered. A sound signal should alert when the road safety system is not in normal position, the sound must start when the booms are lowering.



**Figure 49:** *Level crossing only with light and sound signal*

## 6.2 Level Crossing Motor Current Analysis

The following analysis considers whether an eventual fault in the LC motor-boom infrastructure could be detected by means of current signal analysis.

The barrier machine used in the pilot test is the product „HSM10E“ from the manufacturer „Scheidt&Bachmann“. The current is provided with three batteries in serial (36 Volt) which are charged by a charging rectifier. The current for opening the barriers is about 10-30 A max. (at 36V). Figure 50 shows the normal opening and closing of barrier gates.

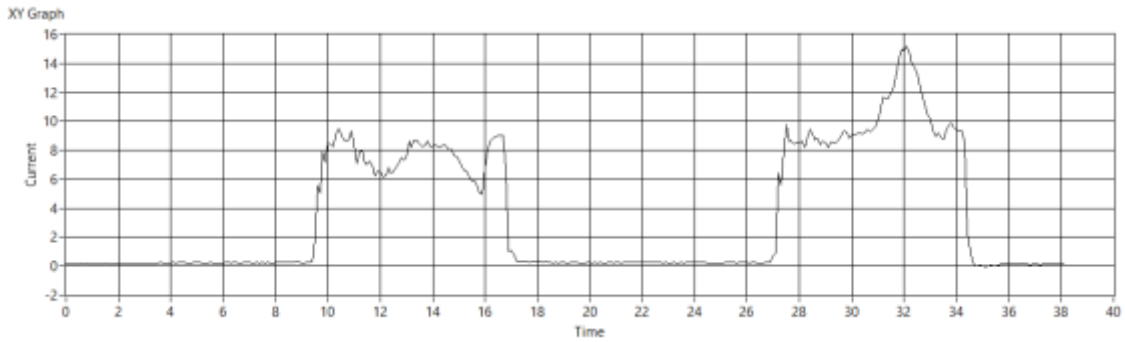


**Figure 50:** Current signals in time domain for a normal opening and closing condition

The current signals gathered are related to different infrastructure scenarios. Six different scenarios have been considered: (1) Normal - Opening of the boom; (2) Normal - Closing of the boom; (3) Opening with no boom attached to the motor; (4) Opening with the boom fastened in the open position; (5) Opening with the boom fastened in the closed position; (6) Opening with the boom fastened at 45 degrees.

Figure 51 shows the current signals in time domain gathered for different infrastructures conditions. Three different signals are gathered for each infrastructure condition. The signal with the highest quality is selected for further analysis.

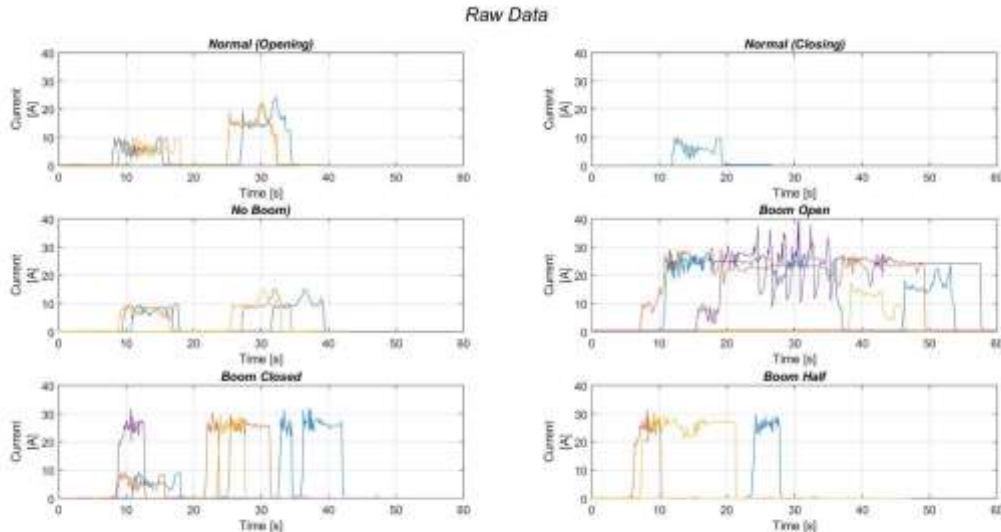


**Figure 51:** Current signals in time domain for different infrastructure conditions

Figure 52 shows the selected signals synchronized in time domain. The signals vary significantly for the different conditions. In the normal infrastructure condition, two main signals are present, each with a different peak value and duration. A generic blockage of the boom, no matter in which position, leads to an increase of mean and peak current levels. No boom leads to a lower mean current level, nevertheless without altering the signal morphology.



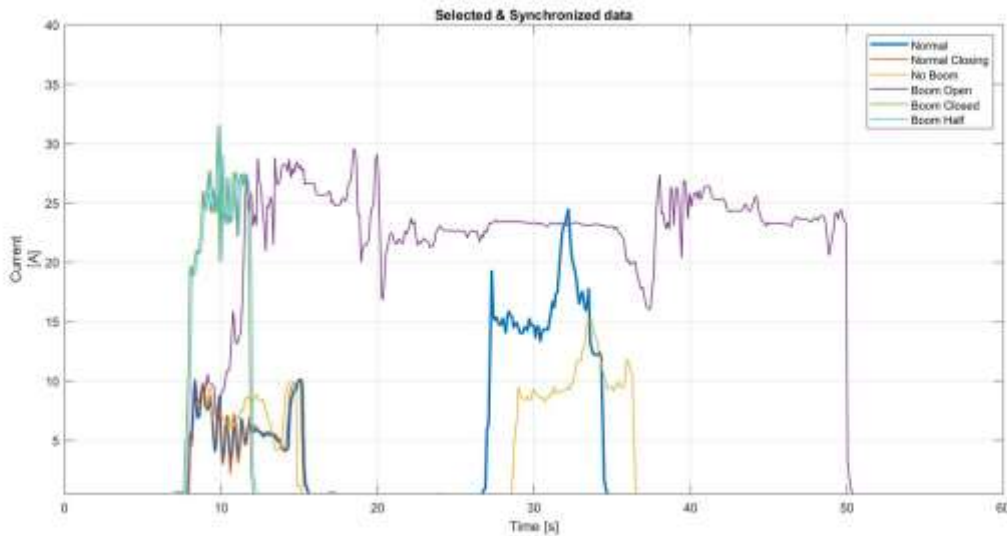


**Figure 52:** Selected and synchronized current signals for different infrastructure conditions.

Table 10 shows the RMS and peak current levels for each infrastructure situation. The RMS and peak values are associated with the two parts of the signal detected. Operationally, the RMS and peak values have been computed in the lapse of time in which the absolute value of the current signal re-turned a higher value than a predefined tolerance, 1 A. For the cases where the boom is locked in position, the peak current level always exceeds the normal value, i.e., 25 A, by about 5 A of difference. No boom leads to a decrease in the current peak level of about 10 A.

**Table 10 :** RMS and peak levels - Current Analysis

Dynamic situation	RMS [ $A_{rms1}$ ]	Peak [ $A_{peak1}$ ]	RMS [ $A_{rms2}$ ]	Peak [ $A_{peak2}$ ]
Normal	6.3976	10.15	15.68	24.48
Normal Closing	6.53	10	–	–
No Boom	7.48	9.91	10.07	15.12
Boom Open	22.86	29.57	–	–
Boom Closed	22.76	31.55	–	–
Boom Half	22.76	31.55	–	–

### 6.3 Traffic signal light current measurement

The road traffic signal was built by RWTH-AACHEN which is not a standard signal for railway purposes. However, for the sake of the experimental work, the mock traffic signal lights were used. The current was measured using a standard ammeter connected in serial. The ammeter gives the reading of the current.

The traffic signal light at the mock LC is made of LEDs. There are 40 LEDs connected in series and in parallel for the yellow blinking signals. The signal light changes from blinking yellow to red in 3 seconds. Four test scenarios have been tested.

Scenario 1. All 40 LEDs working (100% working)

Scenario 2. 10 LEDs are disconnected (75% of LEDs working)

Scenario 3. 20 LEDs are disconnected (50% of LEDs working)

Scenario 4. 30 LEDs are disconnected and only 10 are working (25% of LEDs working)

Current signals for the four scenarios are measured with three repetitions for each scenario. Figure 53 shows the current measurement for the four scenarios, which clearly shows a reduction in the current measurement.

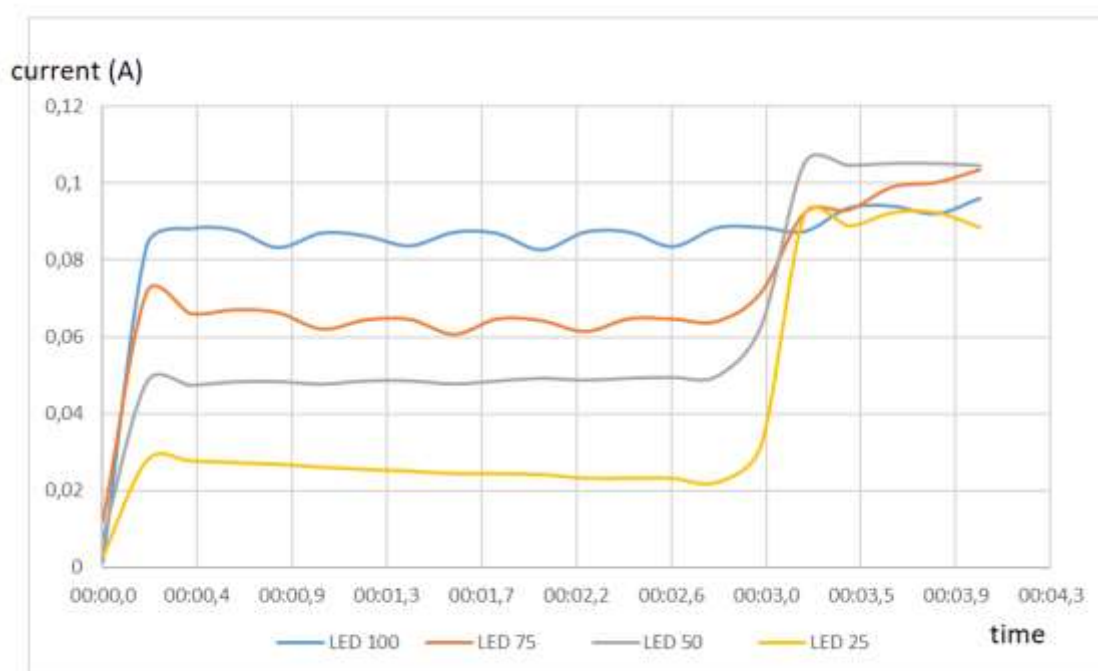


**Figure 53:** Current measurement of traffic signal lights with different percentages of working LEDs



## 7. PRELIMINARY RESULTS FOR CHOSEN SCENARIOS

---

### 7.1 Photogrammetry

Some mock-up tests were conducted and they revealed an issue to detect moving objects with the photogrammetric method. Therefore, a photogrammetric model was created to compare two datasets. In Figure 54, you can see an example for scenario. The main objective is to detect the displacement of the pen with the photogrammetric method. The object was moved between two states (Date 1 and Date 2).



**Figure 54.** *Mock-up with object detection.*

A 3D-model was obtained to compare two sets of pictures (Figure 55). The green areas represent stable zone, yellow depressions and red elevations. These results are consistent with our expectations. A yellow zone of depression can be observed at the old location of the object, and a red zone of elevation at its new location. Although centimetre precision is not enough to show the movement of sand under the object, it would be sufficient for LC application. It was necessary to calibrate camera with photo scan software to improve distortion correction on the edges of the model (Figure 55).

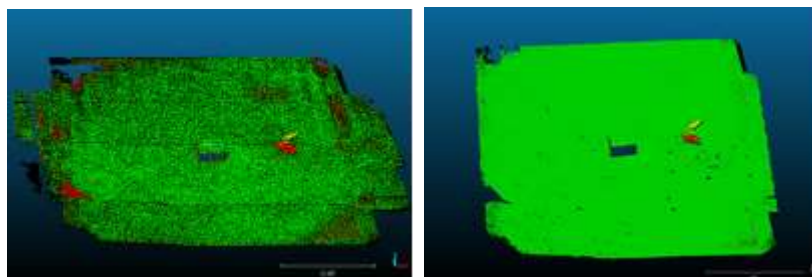


**Figure 55.** *3D photogrammetric models' comparison with object detection. Centimetre precision without calibrate (left) and millimetric precision with calibrate (right).*

Seven photogrammetric models were obtained from a batch of photos. In order to limit the processing time and to prevent software crashes, 260 photos converging towards the surface were used, as seen in the green rectangles in Figure 56, to calculate 3D models with around 25 meters of roadway with adapted focal to obtain a strong density of points.



**Figure 56.** Example of camera device layout for scanning model.

Different photogrammetry software can be used to generate a cloud with photos game. Micmac has been used (Pierrot-Deseilligny et al 2016 [22]) for full model because of the possibility of calibrating the cameras. Three photos are needed to perform the calibration of each camera, in our case photos of geometric shapes were used.

Point clouds must be recalibrated with common repository. The first configuration (1a and 2a') was defined as a reference and therefore must be georeferenced. Two methods were used: GPS points (GCP point in micmac), and the distances method, where the cloud is georeferenced to an absolute reference by similarity.

In Figure 57 and Figure 58, the models with two types of configuration (bump and hollow) is obtained. It shows a top view representation. Each model includes about 25.2 million of points. The geometric dimensions of the study area are 3.57 m by 24.88 m which leads to 25 points per cm<sup>2</sup>.



**Figure 57.** Photogrammetric model – Bump configuration (left to right 0, 3.5 and 7 cm).



**Figure 58.** Photogrammetric model – Hollow configuration (left to right 0, 3, 5 and 5.7 cm).

Each model (file with extension \*.ply) was then compared with CloudCompare against each other in order to obtain 3D comparison model and thus quantify the degradations encountered on the crossing. An example of a model is presented in Figure 59. The direct cloud-to-cloud comparison with the closest point technique does not require gridding or meshing of the data and is the simplest direct 3D comparison. Each point is able to define in both clouds. The surface variation is estimated as the distance between the two points (M3C2). With the length of the measuring area, cutting to three zones is necessary in order to obtain a coherent result. It shows a typical cloud of the surface change with depth.

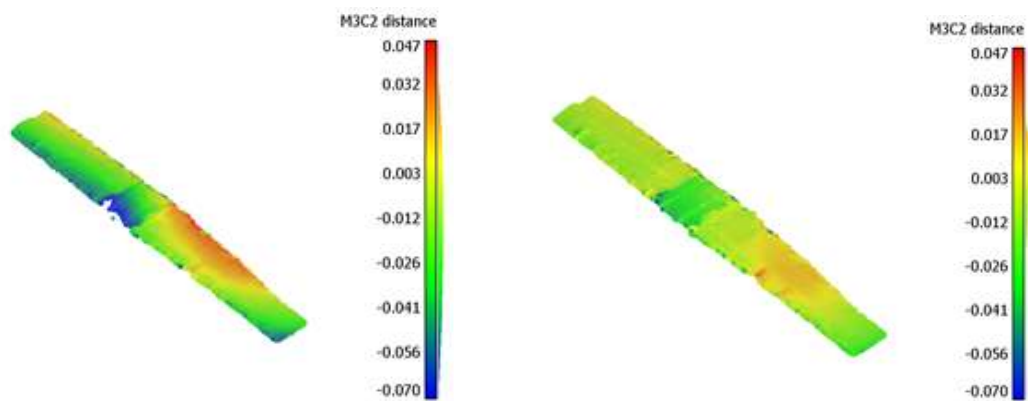


**Figure 59.** Incoherent results full treatment M3C2 (left). Coherent result with cutting and merging zone treatment M3C2 – hollow configuration 2a'-2d' (right).

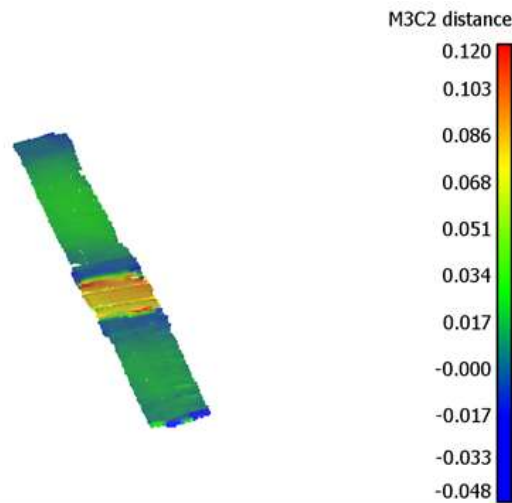


**Figure 60.** Example of 3D photogrammetric model comparison – model bump 0 and 7 cm.

According to Figure 60, the measured distance is sensitive to the cloud's roughness. So, this technique is used for change LC surface on dense clouds. This figure also shows a distance around 8.6 cm on level crossing. It is similar with levelling results. Figure 61 illustrates the depression of the level crossing comparing configuration 1a and 1c.

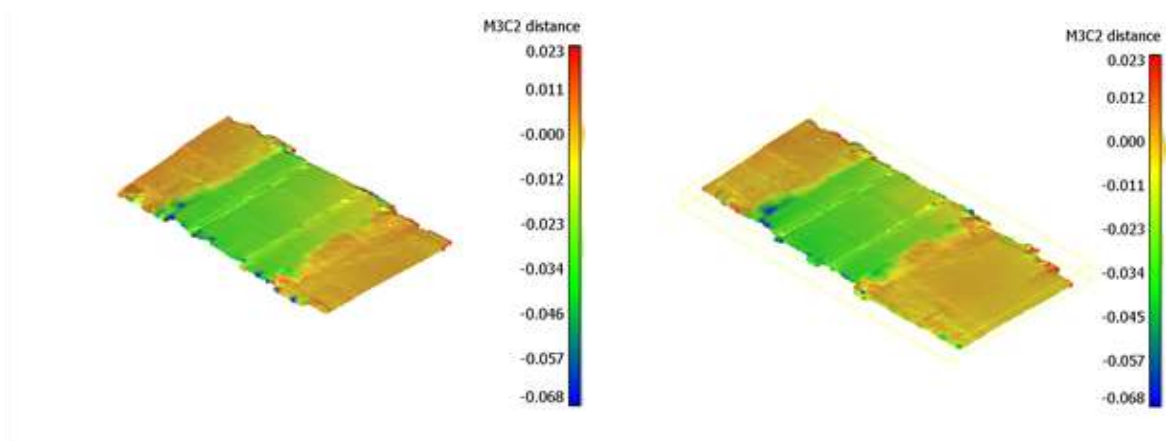


**Figure 61.** Comparison model hollow 2a'-2b' (left). Comparison model hollow 2a'-2d' (right).

From a computer development, we can obtain geometric profile data. The graph below (Figure 63) shows a difference between model bump 0 (blue curve) and model bump 7 (red curve) representative of values obtained with levelling.

Results obtained on the LC central zone for hollow configuration (Figure 61) show more deformation on configuration 2a'–2d' with greater truck passages with a depression marked in wheel passage.

This technique is satisfactory for detecting deformations on level crossing. Application of this technique in the level crossing context is suitable. These results are similar to Lague et al, 2013 [21].

With cloudcompare it is possible to recover manually a geometric profile as shown in Figure 62.

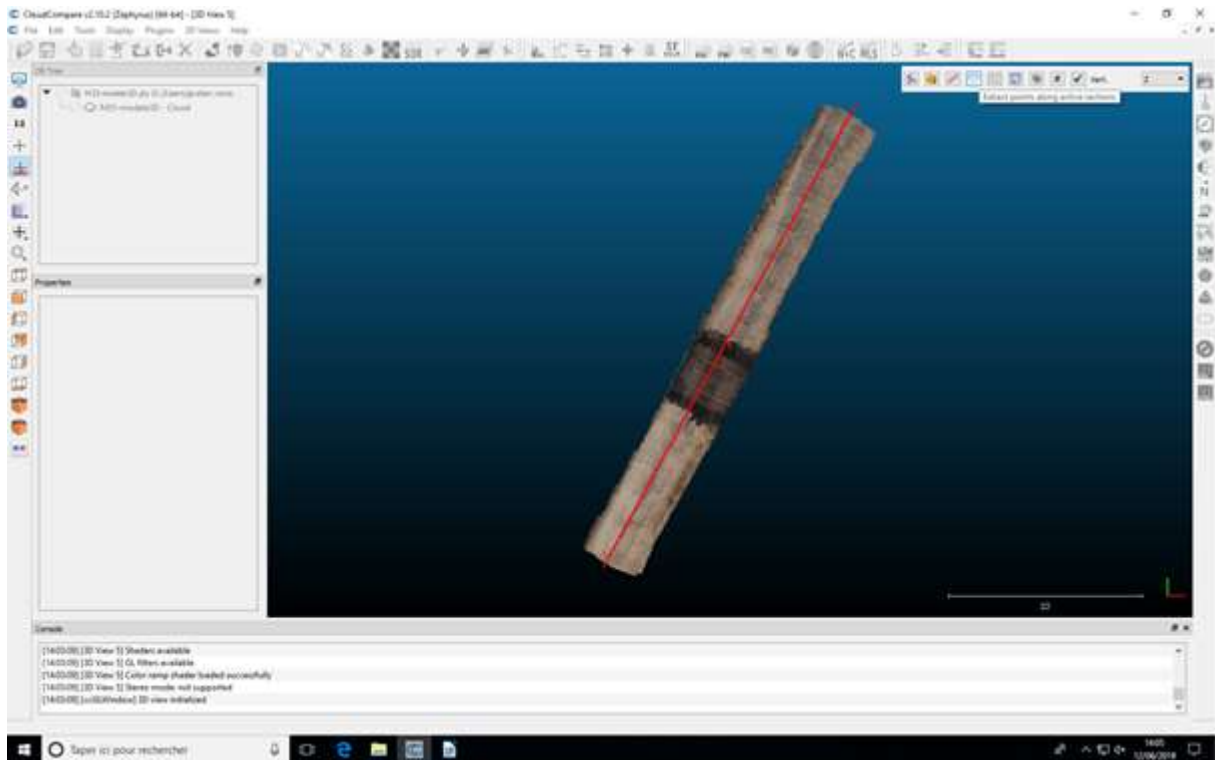


**Figure 62.** Geometric profile recovery with cloud compare.

To complete this treatment, the data of geometric profile recovered were leveraged by an algorithm developed in Python programming language. Figure 63 represents the modality in bump with the configuration at 0 cm in blue and at 7 cm in red. Figure 63 shows a difference between model bump 0 (blue curve) and model bump 7 (red curve) representative of values obtained with levelling. A similar photogrammetric example with another application was described in Fauchard et al 2013 [14] and Chanut et al 2017 [15].

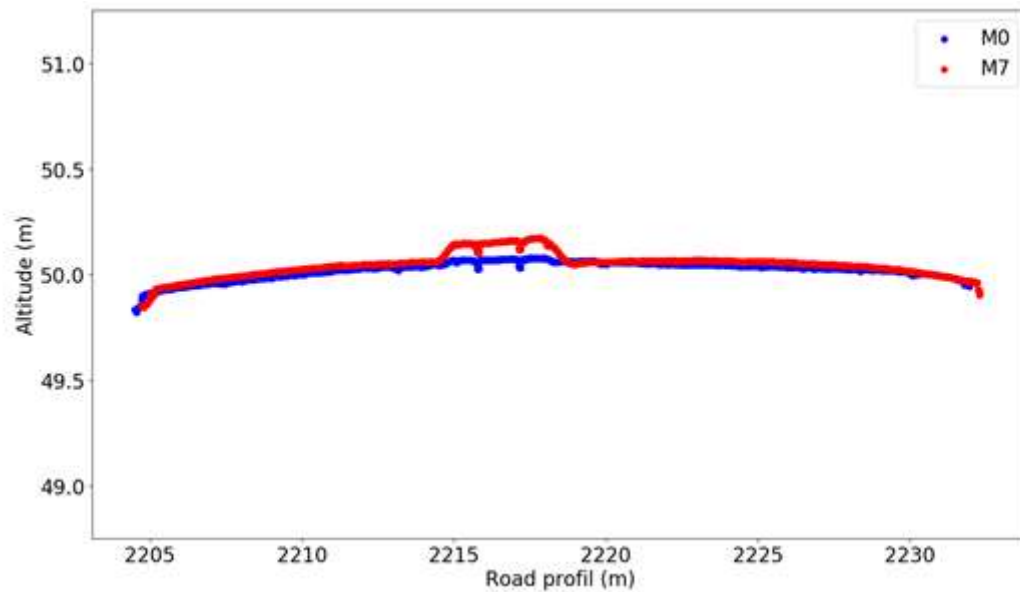


**Figure 63.** Example of geometric profile – model bump 0 and 7 cm.

An approximate surface profile is displayed with the dangerous areas pointed out in red colour

The figures below show that between two different trucks appears a conflict point with a different holder false. The photogrammetric method is used to efficiently detect and locate conflict points according to the characteristics of the truck.

This surface profile depends on truck characteristics as shown in Figure 64.

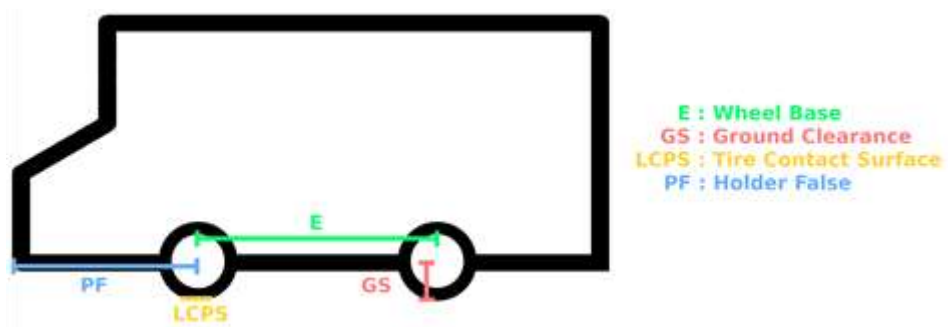


**Figure 64.** Truck characteristics – surface profile.

## 7.2 Vibration (VACC, seismic)

Four passages of the VACC vehicle run over the different configurations and datasets are recorded for each configuration. The average maximum amplitude is considered. Figure 65 presents an example of VACC record average.



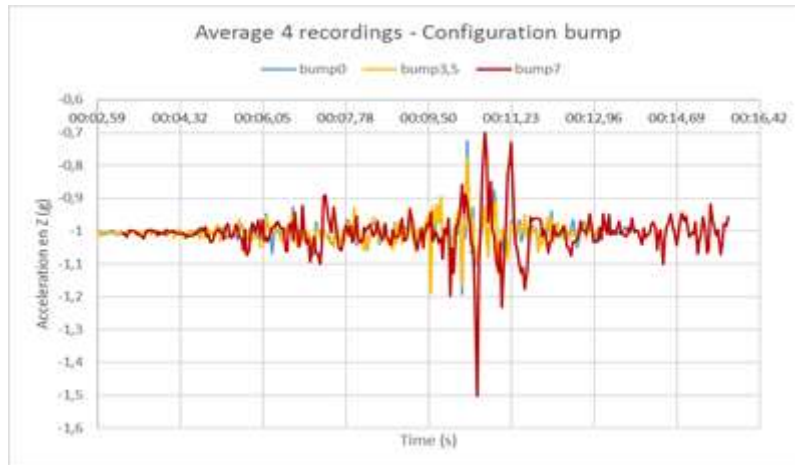


**Figure 65.** Example VACC average - bump configurations.

For any increase of the height of the bump or the hollow, increase of the acceleration is recorded as shown in Figure 66 and Figure 67.

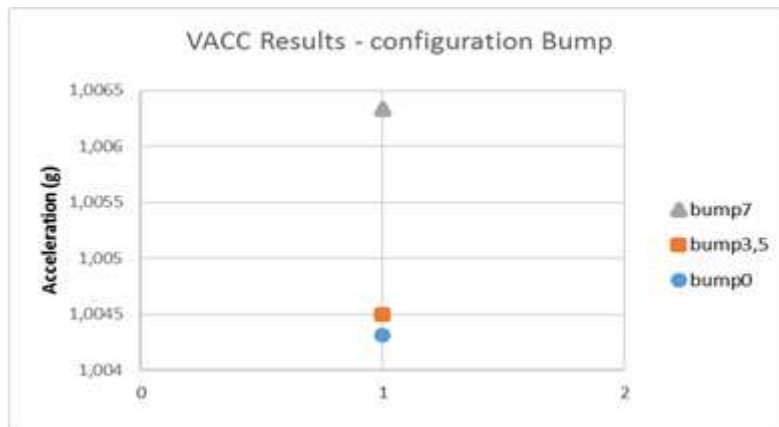


**Figure 66.** VACC results - bump configuration.

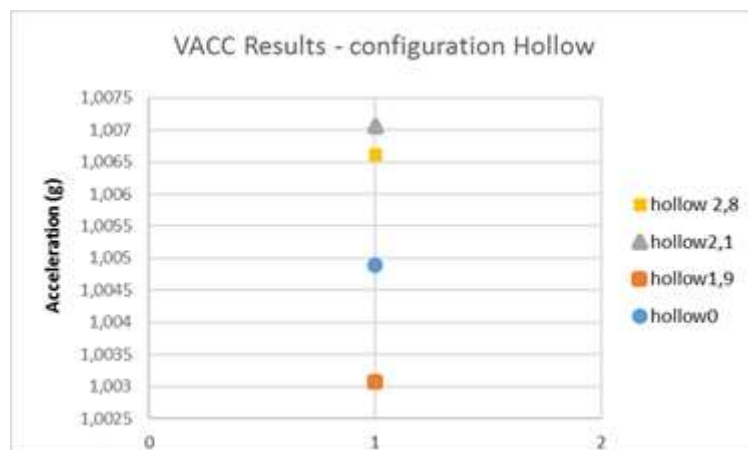


**Figure 67.** VACC results - hollow configuration.

Nevertheless, the variation of the amplitudes remains very small and the result can probably vary according to the lateral deviation of the vehicle on the roadway.

The variation of the acceleration according to the speed and the height of the LC is presented in Figure 68 for a van and in Figure 69 for a truck. For the van, the variation of the acceleration increases when the speed and the height of the level crossing becomes higher. For the truck, results are not representative, as the 3 km/h speed could not be correctly realized. Figure 69 shows anomalies as the acceleration should be varying with a higher value when speed and height of the level crossing increase.

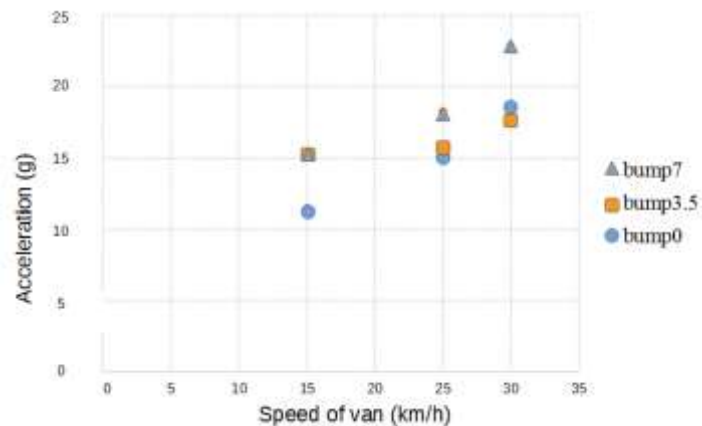


**Figure 68.** Acceleration according to the speed and height of the LC for the van.

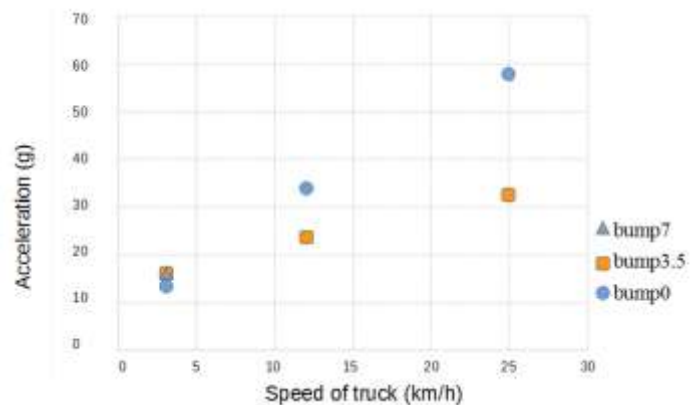


**Figure 69.** Acceleration according to the speed and height of the LC for the truck.

### 7.3 The thermal infrared method: a tool complementary to photogrammetry

This preliminary study aims to assess the potentialities of the thermal infrared method to detect surface cracks. Such cracks may be present on the asphalt in contact with the level crossing which is subject to deformation. More generally, the results obtained during this study may have larger applications and be useful for fissure detection on infrastructures, civil engineering structures, etc... Cracks are usually mapped by « hand » on the ground using visible imagery, a method requiring a considerable amount of time. Semi-automatic mapping methods can be used but remain ineffective when the reflectance of the crack is similar to its environment. For example, a dark crack will be difficult to detect on a dark background,

because of the lack of contrast on the photography. The thermal infrared method allows to map the surface temperatures of an object with a camera (using the relationship between the temperature and the emitted spectral luminance, via the Planck's law). The surface temperatures depend first of all on the thermal inertia of the soil (Watson, 1975) [38]. On a homogeneous surface (like a road, a wall, etc...), the surface temperature may also depend on the orientation of the surfaces to the sunlight. This is why a crack may not have the same temperature than the surrounding material, due to its shape (depending on the time of the day).

In our team, we work on the link between surface temperatures, subsurface processes (associated to water and airflow, evaporation) and surface properties (effect of porosity, thermal conductivity, topography and albedo), at different scales of time and space (Antoine et al., 2009 [34]; Antoine and Lopez, 2018 [36]). In particular, we are now highly interested in understanding the link between the micro-topography and the temperature signal, using a thermal infrared camera. Indeed, the observed surface temperatures may be highly influenced by the presence of topography, inducing temperature contrasts of several degrees Celsius and depending on the sky proportion  $\alpha$  (Figure 70).

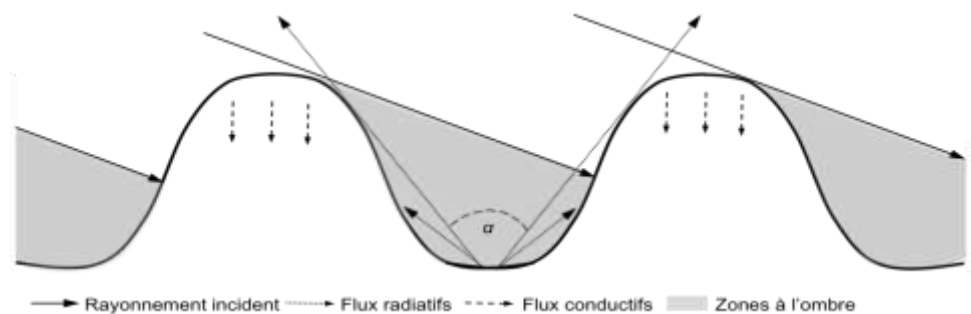


**Figure 70.** Influence of the topography on the radiation. The emitted energy seem by a thermal infrared camera highly depends on the sky proportion  $\alpha$  (Antoine et al., 2017 [35])

We have extended the one-dimensional conductive-radiative numerical code developed in Antoine et al., 2009 [34] to characterize the spatio-temporal thermal behaviour of a centimetric fissure in two dimensions, (Figure 71. 2D numerical modelling of the thermal behavior of a surface fracture. a) Temperature evolution on a diurnal cycle at the surface, 10 cm, 20 cm, 30 cm and 50 cm depth outside the surface fracture b) 2D temperature pattern within a fissure embedded in a homogeneous soil and c) spatial temperature variation within a fissure, from its summit to its center at depth.). This code (implemented with Comsol Multiphysics) is fully based on the physical and optical characteristics of our previous 1D code (radiative surface boundary conditions, introduction of a 2D sky view parameter in the Stefan-Boltzman law, associated to the micro-topography). Currently, our modelling only takes into account E-W fissures, with sides receiving (and thus re-emitting) the same energy amount during the diurnal cycle.

*Figure 71a* shows an example of the temperature evolution of the soil during a diurnal cycle and at different depths (0 cm, 10 cm, 20 cm, 30 cm, 50 cm). It shows a typical attenuation of the thermal front with depth, with a phase shift of the signal depending on the thermal diffusivity of the medium. These results are similar to Watson, 1975 [38] and Antoine and Lopez, 2017 [36].

*Figure 71b* displays the spatial temperature variation within the fissure just before sunrise. This figure illustrates the cooling delay of the fissure during the night: as the sky view parameter is lower in the fissure compared to the surrounding plane surface, the amount of emitted energy within the structure is lower. As a consequence, the cooling is delayed within the fissure and the later appears hotter before sunrise. Such contrast may be inverted during daytime, depending on the thermal inertia of the surface material.

The

*Figure 71 c* shows the spatial thermal variation at the surface of one side of the fissure with a non-linearly increases of the temperature by more than 2°C up the centre of the fissure. Such thermal contrast should allow the detection of fissures using current commercial thermal cameras which have sensitivities better than 50 mK.

This theoretical thermal pattern may be clearly observed in the *Figure 72*, representing several fissures on a road (*Figure 72a*), observed in the morning in winter (with a FLIR Vue Pro embedded on a DJI Phantom 4 UAV at 2 m height): the dark crack system is seen to appear warmer than the surrounding soil by approximately 2°C (*Figure 72b*). This phenomenon may be due to the micro-topography of the network, but also to the reflectance. Indeed, as they are darker, the fissures should effectively appear warmer than the surrounding during daytime. Interestingly, when analysed in detail, some fissures have a low reflectance similar to the road, but however still appear warmer (white square in *Figure 72a*). This last observation shows 1) that the micro-topography may play a major role in the surface temperature of the fissure network (more than reflectance) and 2) that the thermal infrared method may be complementary to the visible imagery for the detection of a fissure network, even in low reflectance areas.

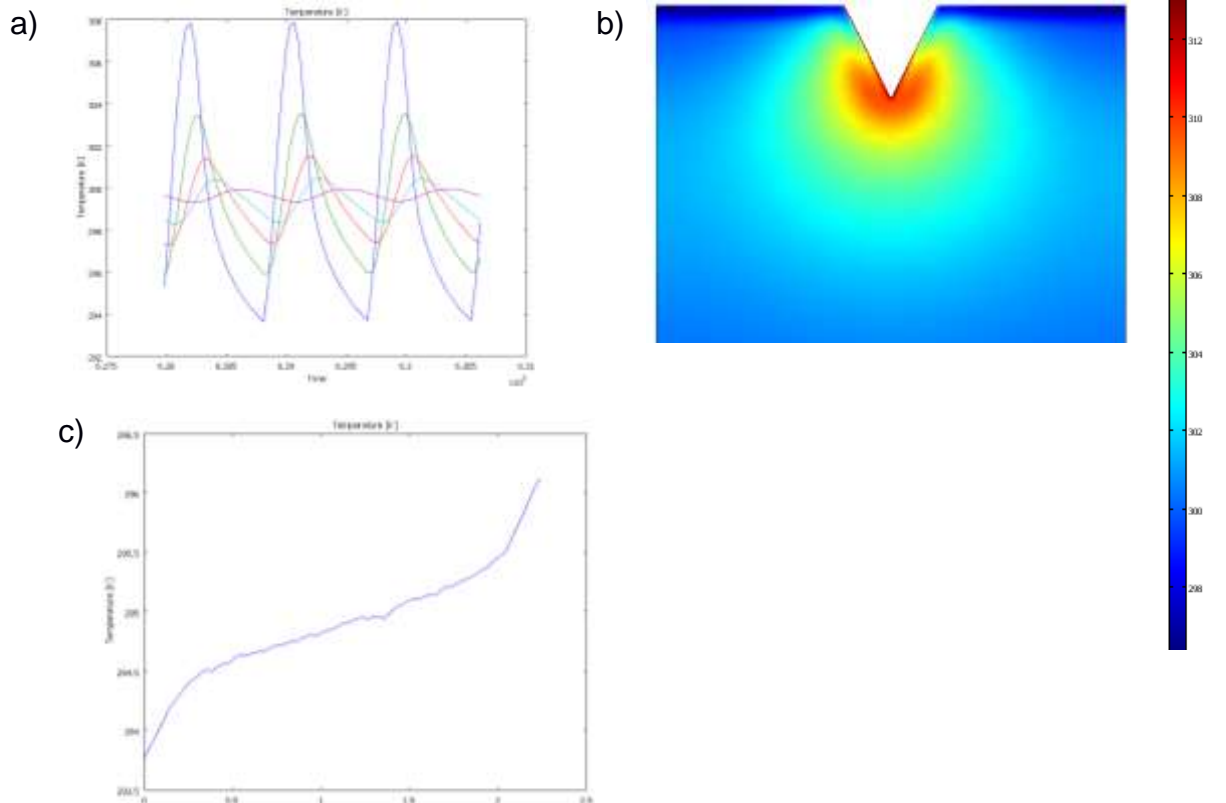


**Figure 71.** 2D numerical modelling of the thermal behavior of a surface fracture. a) Temperature evolution on a diurnal cycle at the surface, 10 cm, 20 cm, 30 cm and 50 cm depth outside the surface fracture b) 2D temperature pattern within a fissure embedded in a homogeneous soil and c) spatial temperature variation within a fissure, from its summit to its center at depth.

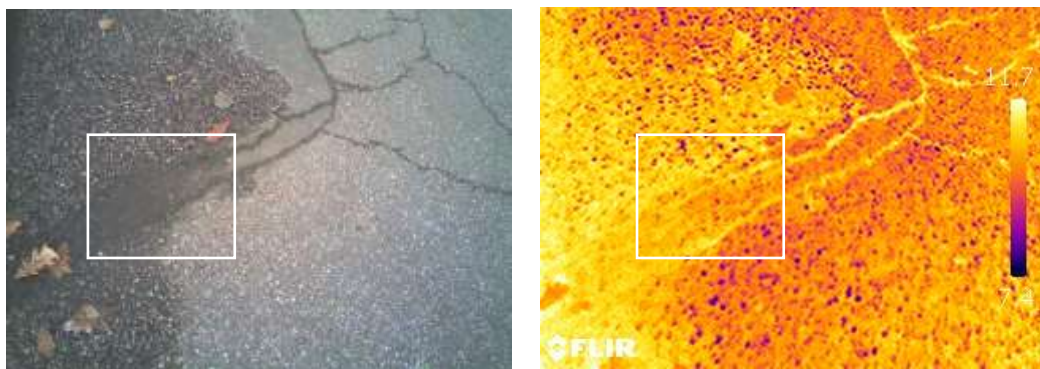


**Figure 72.** a) Photography of thin fractures on a road during the morning in winter; b) Thermal infrared observation of the same area. Note 1) the temperature contrast between the fractures and the surrounding medium and 2) the distinct thermal pattern of the fissure network, even in areas with similar reflectance.

This study aimed to detect potential cracks appearing on the asphalt in contact with the LC, when the structure is being deformed. Our hypothesis was 1) that this asphalt may be subject to cracking at the contact of the deformed LC and 2) that the cracks may be detectable using the thermal infrared method during daytime. The experiment (discussed in the photogrammetric section) consisted in triggering deformations of the LC by repeated passings using a car and a truck. After each passing, the thermal infrared method was applied on the two asphalt bands in contact with the LC. The methodology consisted of acquiring thermal images and photos using a high-resolution thermal camera available (Variocam HD 800, 1024\*768 pixel) at 1 m height. The 8 Mp visible camera is directly present on the thermal infrared camera. These data were then used to obtain 3D visible and temperature maps calculated using the photogrammetric method. In this case, the 3D modelling enriches the data, bringing a topographic (depth) information in addition to the temperature and visible reflectance. Here, we only present preliminary results (general model + one passing after fracturing), as the CER experiment was performed in June 2019. It will be of interest to continue with measurements on different tests site. Figure 73 displays the 3D general temperature map of the LC obtained using the thermogram metric method (developed in our team) and obtained at 10 a.m., i.e. during the warming of the structure. Due to their high thermal inertia (important thermal conductivity, density and heat capacity), the railways are 7°C colder than the surrounding environment during the morning (while it may appear warmer during the night). It is of note that the two asphalt bands in contact with the LC do not have the same temperatures. The asphalt band A1 is clearly warmer than A2 during the morning (*Figure 73* with contrast of 3°C). This observation should be associated to a difference in thermal inertia and thus to a contrast in the compaction degree of the bands: these structures were built just before the experiment, but within an interval of several days for A1 and A2.

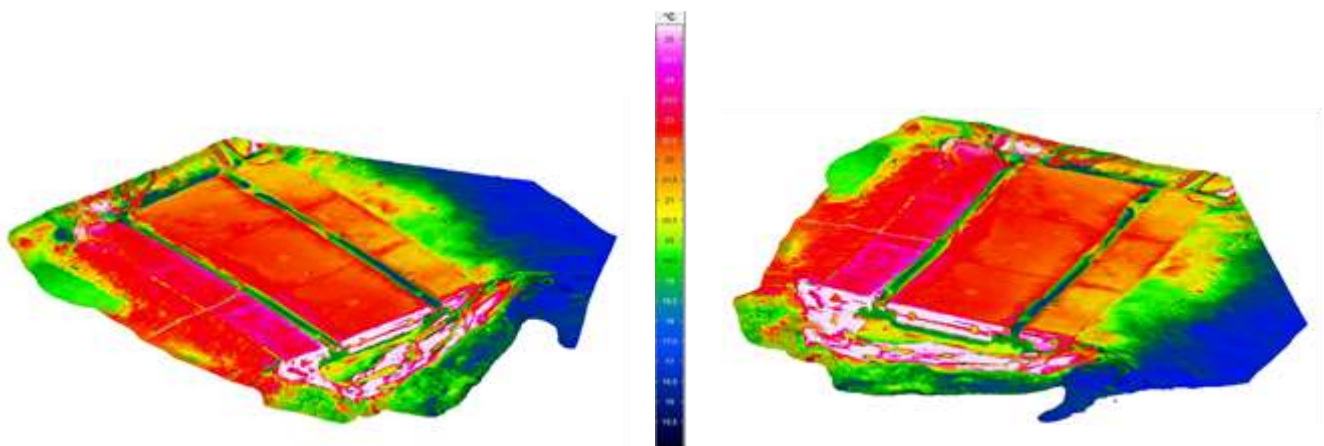


**Figure 73.** Different views of the general 3D temperature map of the LC using the thermogram metric method (A1 view from the left and A2 view from the right).



Figure 74 exhibits an example of 3D thermal and visible map on A1 after three crossings (car + truck). First, a crack is induced within the asphalt band A1 (white square, Figure 74, a), due to the subsidence of the LC. Second, a temperature variation is detected in this area, associated to the recent crack formation (Figure 74, b). In this case, the temperature contrast is 2°C between the fissure and the surrounding area, while the crack may be highly difficult to detect with semi-automatic segmentation algorithms in the visible wavelength. More work will be obviously done in the next months to characterize the thermal behaviour of the fissure for all the crossings. However, from all these results, we plan to combine the visible, thermal and depth information to enhance some crack detection algorithms. The work will have to be continued in a second time.

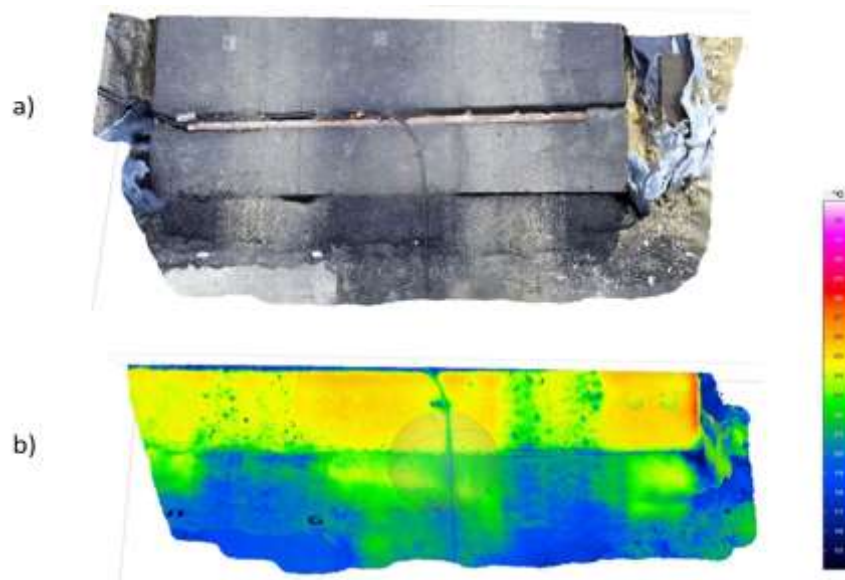


**Figure 74.** a) 3D visible model of A1 (view from the top) and formation of a crack due to the LC deformation (white square) and b) 3D temperature model (view from the bottom) of the A1 Asphalt band. Note the presence of the thermally distinct crack recently formed during the deformation of the LC.

## 8. CONCLUSIONS AND NEXT STEPS

---

The deliverable of task 3.3 is essentially dedicated to avoiding collisions at LCs between trains and heavy vehicles which are prone to stuck at LCs through informing (especially those exceptional transport vehicles) the geometrical limits and requirements for a safe running over the specific LC. The tested measures are interesting for assessing the level of LC infrastructure condition and for informing owners when it's necessary to maintain it.

This measure was applied on a level crossing mock-up installed on Rouen test site. The mock-up represented a LC in which different scenarios of infrastructure were played. The monitoring system ensured the safety performance of the LC through the continuous and real time monitoring through two approaches:

- Vibration sensors were installed on the relevant track/road components and data was collected to set alert threshold to the LC operator. The PSD response of measured vibrations were used to identify and to qualitatively detect alarm levels.
- A photogrammetric device was used to monitored infrastructure surface condition and to detect any deterioration of the structure. This system could also measure displacement and deterioration of the road surface. In addition, the visible information combined to thermal infrared data to enhance the interpretations of the potential disorders as cracking. High permeability zones generated a thermal anomaly of several degrees.

The methods tested at Cerema aim to provide managers with efficient means to monitor structural and geometric LC state and to ensure preventive maintenance and safety for level crossing. The vibration method is particularly appealing for its cost-effectiveness and the reliability of the acceleration data.

These methods have shown their effectiveness in detecting and quantifying a geometric evolution. However, they need to be improved and industrialized in order to be easily used by infrastructure managers.

Each method has advantages and disadvantages described in **Erreur ! Source du renvoi introuvable.**

Table 11 Advantages and disadvantages of tested measures in task 3.3

Methods	Advantages	Disadvantages
Photogrammetry (vehicle instrumented with cameras)	<ul style="list-style-type: none"> <li>- geometric modeling with realistic rendering of the LC to determine possible evolutions</li> <li>- low cost of the measurement device</li> </ul>	<ul style="list-style-type: none"> <li>- measurement preferably in cloudy weather condition and on dry pavement</li> <li>- significant processing time depending on the quality of the result sought</li> <li>- programming of measurement campaigns.</li> </ul>
Vibration of LC (fixed accelerometers on LC)	<ul style="list-style-type: none"> <li>- a permanent real-time LC monitoring allowing an alert for the maintenance department or blocking traffic with detected danger</li> </ul>	<ul style="list-style-type: none"> <li>- Need to instrument the LC and to set up a communication device with a control post. Relatively high cost of deployment</li> </ul>
VACC (accelerometers included inside vehicle)	<ul style="list-style-type: none"> <li>- Only one vehicle is necessary for periodic monitoring of the evolution of LCs in a network.</li> <li>- Vehicle not specifically dedicated</li> </ul>	<ul style="list-style-type: none"> <li>- Necessary to set acceleration thresholds beyond which geometry measurements must be made on the LC in order to confirm the level of evolution of the LC</li> <li>- Programming of measurement campaigns</li> </ul>
Infrared thermography (manual thermal measurement)	<ul style="list-style-type: none"> <li>- Early detection of a structural evolution of the LC.</li> <li>- Low cost</li> </ul>	<ul style="list-style-type: none"> <li>- Rapid detection of deformation can lead to the appearance of a conflict zone.</li> <li>- Programming of measurement campaigns</li> </ul>

Different techniques implemented on full scale in Cerema test site can be implemented to ensure LC safety in the area of conflict prevention between the structure and a vehicle.

However, each technique has advantages and disadvantages. It will be necessary choose the implemented technique depending on the budget, the dangerousness of the LC, the evolution speed according to the geometric structure.

Photogrammetry allows periodic monitoring, the measurement accuracy of which can be adapted as required.

Fixed accelerometers with a relatively high implementation and exploitation cost is justified when it is necessary to monitor the evolution of a LC in real time.

Mobile accelerometers, which is cheaper than photogrammetry, allows periodic monitoring but requires additional measurements after detecting threshold overshoot.

Infrared thermography is justified only by the need for early detection of the degradation of the transition zone to the railway structure.

## 9. BIBLIOGRAPHY

---

- [1] News weblink: [<https://www.independent.co.uk/news/truck-train-crash-video-georgia-railway-us-accident-crossing-a8286911.html>]
- [2] SAFER-LC – Deliverable D1.1
- [3] **Cirovic G., Pamucar D.**, “Decision support model for prioritizing rail-way level crossings for safety improvements: Application of the adaptive neuro-fuzzy system,” *Expert Systems with Applications*, vol. 40, Issue 6, pp. 2208 – 2223, 2013.
- [4] **Starcevic M., Baric D., Pilko H.**, “Safety at Level Crossings: Comparative Analysis,” *CETRA 2016*, 2016.
- [5] News weblink: [<https://www.dailymail.co.uk/news/article-5764973/One-dead-16-injured-train-ploughs-truck-northern-Italy.html>]
- [6] **Wang T.**, “3D Infrastructure Condition Assessment For Rail Highway Applications”, University of Kentucky, 2016, Doctoral dissertation, Theses and Dissertations—Civil Engineering. 41
- [7] weblink: [<https://oli.org/track-statistics/collisions-casualties-year>]
- [8] SAFER-LC – D1.3. Needs and requirements for improving level crossing safety
- [9] News weblink: [<https://news.sky.com/video/train-smashes-through-fedex-lorry-at-utah-crossing-10741786>]
- [10] *Geometric Design of Highways and Streets (the Green book)*, American Association of State Highway and Transportation Officials (AASHTO), 2011.
- [11] *American Railway Engineering and Maintenance-of-Way Association (AREMA) Manual for Railway Engineering (AREMA)*, 2015.
- [12] **Baqersad, J., Poozesh, P., Niezrecki, C. and Avitabile, P.**, *Photogrammetry and optical methods in structural dynamics – A review*, *Mechanical Systems and Signal Processing*, 86, 2017, 17 - 34.
- [13] **Wikipédia** in **French**, Photogrammetric article: <http://fr.wikipedia.org/wiki/Photogramm%C3%A9trie>
- [14] **Fauchard C. Antoine R., Bretar F., Pierrot Deseilligny, M., Dupont J.P., Fargier Y., Lacogne J., Guibert V., Margerie P., Therain P.F., & Maisonnave C.**,(2013) Assessment of an ancient bridge combining geophysical and advanced photogrammetric methods: Application to the Pont De Coq, France. *Journal of Applied Geophysics*.

- [15] **Chanut, M-A., Kasperski, J., Dubois, L., Dauphin, S. & Duranthon, J-P**, Quantification des déplacements 3D par la méthode PLaS - application au glissement du Chambon (Isère), *Rev. Fr. Geotech.*, **2017**, 4
- [16] **Brunier, G., Fleury, J., Anthony, E. J., Gardel, A. & Dussouillez, P.**, Close-range airborne Structure-from-Motion Photogrammetry for high-resolution beach morphometric surveys: Examples from an embayed rotating beach, *Geomorphology*, **2016**, 261, 76 - 88
- [17] **Dietrich, J. T.**, Riverscape mapping with helicopter-based Structure-from-Motion photogrammetry *Geomorphology*, 2016, 252, 144 - 157
- [18] **Neffra, M.**, *Aerial and Close-Range Photogrammetric Technology: Providing Resource Documentation, Interpretation, and Preservation*, 2009.
- [19] **Jalandoni, A., Domingo, I. & Tañón, P. S.** Testing the value of low-cost Structure-from-Motion (SfM) photogrammetry for metric and visual analysis of rock art, *Journal of Archaeological Science: Reports*, **2018**, 17, 605 - 616
- [20] **Leon, J., Roelfsema, C. M., Saunders, M. I. & Phinn, S. R.** Measuring coral reef terrain roughness using Structure from Motion close range photogrammetry *Geomorphology*, **2015**, 242, 21 - 28
- [21] **Lague, D., Brodu, N. & Leroux, J.**, Accurate 3D comparison of complex topography with terrestrial laser scanner: Application to the Rangitikei canyon (N-Z), *ISPRS Journal of Photogrammetry and Remote Sensing*, **2013**, 82, 10 - 26
- [22] Pierrot-Deseilligny, M., anonymous, 2016. Micmac documentation : MicMac, aperiodedenis, pastis and other beverages in a nutshell URL <http://logiciels.ign.fr/?-Micmac,3->
- [23] **Barolli L, Zhang M, Wang XA**, Advances in internetworking, Data & web technologies : the 5<sup>th</sup> international, 2017, p 477-487
- [24] **Curt G.**, presentation on photogrammetric device [https://www.sfpt.fr/wp-content/uploads/2016/03/20160317\\_10\\_SFPT\\_G-Curtpresentation\\_SFPT.pdf](https://www.sfpt.fr/wp-content/uploads/2016/03/20160317_10_SFPT_G-Curtpresentation_SFPT.pdf)
- [25] **Helfrick, M. N., Niezrecki, C., Avitabile, P. and Schmidt, T.**, *3D digital image correlation methods for full-field vibration measurement*, Mechanical Systems and Signal Processing, 25, 2011, 917 - 927.
- [26] **Amaneh E. Kenarsari, Stanley J. Viton, John E Beard**, *Models of tractor tire footprints using close-range digital photogrammetry*, Journal of Terramechanics 74 (2017) 1-11
- [27] **Lee, Y., et al.**, "Implementation of Accelerometer Sensor Module and Fall Detection Monitoring System based on Wireless Sensor Network". 2007. <<http://cdn.intechweb.org/pdfs/16358.pdf>>.

- [28] **Tiwari A., Prasanna B., Frank L.L.**, "Energy-efficient wireless sensor network design and implementation for condition-based maintenance". *ACM Transactions on Sensor Networks*. 3: 1, 2007. doi:10.1145/1210669.1210670.
- [29] **Bilsova A., Bilos J.**, "Vibration Diagnostics," VSB-TUO: InterDV, registrační číslo projektu, 2012.
- [30] **Rogers M. J. B., Hrovat K., McPherson K.**, "Accelerometer Data Analysis and Presentation Techniques," Tal-Cut Company at NASA Research Center, 1997.
- [31] **Stoica P., Moses R.**, "Spectral Analysis of Signals," *Prentice Hall*, 2004.
- [32] **Rieke F.**, "Spikes: Exploring the Neural Code (Computational Neuro-science)", *A Bradford Book*, 1999.
- [33] Honeywell International Inc., "Honeywell Radar Scanner, Advantages and Benefits," , 2012.
- [34] **Antoine, R., Baratoux, D., Rabinowicz, M., Fontaine, F., Bachèlery, P., Staudacher, T. & Finizola, A.** (2009). Thermal infrared image analysis of a quiescent cone on Piton de la Fournaise volcano: Evidence of convective air flow within an unconsolidated soil. *Journal of Volcanology and Geothermal Research*, 183(3-4), 228-244.
- [35] **Antoine, R., Finizola, A., Lopez, T., Baratoux, D., Rabinowicz, M., Delcher, E., & Staudacher, T.** (2017). Electric potential anomaly induced by humid air convection within Piton de La Fournaise volcano, La Réunion Island. *Geothermics*, 65, 81-98.
- [36] **Antoine R., Lopez T** (2017). Télédétection dans l'infrarouge thermique, Manuel de mécanique des roches, Tome V : Thermomécanique des roches, pp. 157-202, ISBN 978-2-3567-465-7, Paris, Presse des Mines, Collection Sciences de la Terre et de l'Environnement, 2017.
- [37] **Mahrer, Y.** (1982). A theoretical study of the effect of soil surface shape upon the soil temperature profile. *Soil Science*, 134(6), 381-387.
- [38] **Watson, K.** (1975). Geologic applications of thermal infrared images. *Proceedings of the IEEE*, 63(1), 128-137.



